Long-term acid generation and heavy metal leaching from the tailings of Shimokawa mine, Hokkaido, Japan: Column study under natural condition

Kimleang Khoeurn[a,c,*], Asumi Sakaguchi[a], Shingo Tomiyama[b] and Toshifumi Igarashi[b,]

[a] *Sustainable Resources Engineering, Graduate School of Engineering, Hokkaido University, Sapporo, 060-8628, Japan*
Tel.: +81-80-1877-3676
Fax: +81-11-706-6309

[b] *Sustainable Resources Engineering, Faculty of Engineering, Hokkaido University*

[c] *Department of Chemical Engineering and Food Technology, Institute of Technology of Cambodia, Russian Conf. Blvd., Phnom Penh, Cambodia*

**E-mail:khoeurnk@yahoo.com*

ABSTRACT: The leaching from mine tailings results in contamination of nearby groundwaters and rivers by hazardous metals like copper (Cu), zinc (Zn), and iron (Fe). In this study, unweathered tailings samples at depths of 1 to 3 m were collected from a tailings dam of an abandoned mine located in the north of Hokkaido, Japan. The mechanisms of long-term tailings weathering were assessed through leaching of hazardous metals by three column experiments. Measurements of mineralogical and chemical constituents, observation by scanning electron microscopy with energy dispersive X-ray spectroscopy (SEM-EDX), sequential extraction of the tailings, and chemical analyses of the leachates were carried out to determine the processes responsible for the leaching of Cu, Zn, Fe, and sulfate ion (SO_4^{2-}). The contents of Cu, Zn, and Fe in the tailings were mainly associated with ion exchangeable and sulfide fractions. The pH values of the effluents from the columns were 3.0–3.7 throughout the experiments over 84 weeks, and approximately 15-23% of Cu, 35-45% of Zn, 2.5-4% of Fe and 15-20% of S were leached. Higher concentrations of Cu, Zn, Fe, and SO_4^{2-} at the beginning of the experiments were observed, which could be attributed to the dissolution of soluble sulfate minerals present in the tailings. This indicates that the formation and dissolution of secondary soluble sulfate minerals contributed to Cu and Zn leaching. The continuous leaching of Cu, Zn, Fe, and SO_4^{2-} suggests the oxidation of pyrite and other sulfide minerals. During these processes, ferrihydrite, goethite, lepidocrocite, and maghemite were formed and these minerals also acted as a sink for Cu and Zn by adsorption, and/or co-precipitation. These results mean the significance of the long-term behavior of hazardous metals released from mine tailings dams, which could provide helpful information on the management of tailings dams after mine closure.

Keywords: Unweathered tailings, column leaching tests, hazardous metal mobilization, sulfide oxidation, geochemical modeling

Highlights

- Released hazardous metals corresponded to exchangeable fraction/soluble salts at the

beginning of the experiments and subsequent continuous oxidation of sulfide fraction.

- Zinc was more mobilized than Cu and Fe in the tailings.
- Factors affecting pyrite oxidation were not only dissolved oxygen presented in distilled water but also atmospheric oxygen and ferric iron.
- The precipitation of secondary minerals (Fe-oxyhydroxides) was observed.
- The acid mine drainage containing hazardous metals was expected to be released for a long period of time.

1. Introduction

The minerals that represent economically valued ores are chemically stable under in situ geological conditions (Paul et al., 2002). However, these solid phases become unstable when they are excavated and exposed to the atmosphere. Mining and milling processes (i.e., crushing, grinding, washing, etc.) generate four major categories of wastes and wastewater, i.e., (i) mine waste (low-grade ore, overburden, and barren rocks), (ii) tailings, (iii) dump heap leach and (iv) acid mine drainage (AMD). These wastes are disposed to the surrounding land and water body in more or less an environmentally acceptable manner (Shu et al., 2001; Paul et al., 2002; Schuwirth et al., 2007; Zhang et al., 2016).

Large quantities of tailings have been disposed to the environment by past and present-day mining and processing activities. Mine tailings have potential to release significant quantities of metals to water and soils (Moncur et al., 2009; Modabberi et al., 2013) because tailings contain significant amounts of pyrite (FeS_2) and other metal-bearing sulfides, oxide, and silicate minerals, as well as processing compounds (Lindsay et al., 2015).

Acid mine drainage is primarily released during the weathering of pyrite in a solution containing dissolved oxygen. The AMD with metal ions represents significant environmental hazards to freshwater resources. In addition, weathering and oxidation of sulfide minerals contained in the tailings, especially in unsaturated layers, can produce acidic water laden with high concentrations of iron (Fe), sulfate ion (SO_4^{2-}) and potentially hazardous trace metals and metalloids such as arsenic (As), cadmium (Cd), copper (Cu), lead (Pb) and zinc (Zn) (e.g., Olyphant et al., 1991; Benzaazoua et al., 2003; Khorasanipour et al., 2011; Cheong et al., 2012; Goumih et al., 2013). Moreover, the variation in drainage quality from tailings impoundments is mainly a function of grain-size distribution and compositional variations (e.g., iron-sulfide and carbonate-mineral contents) within individual mine-rock lithologies, local climatic conditions, and the presence of microorganisms (Ardau et al., 2009).

Precipitation of the widespread secondary solid phases like evaporative and secondary phases is

another important consequence of weathering and oxidation of tailings (Flohr et al., 1995; Nordstrom, 2011; Carbone et al., 2013). Some of these secondary phases like efflorescent salts are often very soluble and represent only a temporary host for a variety of metals (Frau, 2000; Jambor et al., 2002; Buckby et al., 2003; Hammarstrom et al., 2005), while others such as ochreous precipitates represent a more stable sink for hazardous metals and reduce metal mobility through adsorption or co-precipitation.

Although climate conditions provide fundamental control of many reactions, such as weathering intensity, secondary mineral formation, and the mobility of hazardous metals from tailings (Olyphant et al., 1991; Dold, 1999; Dold and Fontboté, 2001; Dold, 2003; Redwan and Rammlmair, 2012), the mobility of metals from tailings may be different depending on the type of tailings. Numerous research studies have been conducted on the behavior of the metals from tailings, e.g., sulfide-rich tailings, and non-sulfide tailings, both in situ and laboratory observation (Smuda et al, 2007; Yeheyis et al., 2009; Goumih et al., 2013; Root et al., 2015; Kandji et al., 2017; Wang et al., 2017). Laboratory experiments are also required prior to the disposal of mine wastes. This is because rates of acid-producing and acid-neutralizing mineral dissolution in the laboratory are sufficiently similar to those in the field to apply the laboratory results to predictive models of full-scale waste piles (Jurjovec et al., 2002; Benzaazoua et al., 2003; Álvarez-Valero et al., 2009; Kandji et al., 2017).

A closed mine site in Hokkaido has generated AMD for more than 40 years. Mine tailings were the major source of Cu, Zn, Fe, and SO_4^{2-} (Khoeurn et al., 2018). Thus, the AMD has been treated with calcium hydroxide ($Ca(OH)_2$) before the effluents are discharged into the nearby river. However, the treatment period remains unclear and leaching behavior of hazardous metals in the dam is not well understood. Understanding how physical, geochemical, mineralogical, and biological processes control mobility, bioavailability, and toxicity of hazardous metals is important in minimizing environmental impacts on ecosystems including humans and other biotas. Unfortunately, little information is known about the transformation of minerals and mobility of related metals in the tailings. The aim of this research is to investigate the changes in mineralogy and geochemistry of the tailings, to evaluate long-term leaching behaviors of hazardous metals like Cu and Zn from the tailings due to weathering processes with different irrigated rainfalls, and to identify releasing fractions of the metals. The results of this study will help to improve remediation and management system after mine closure. At the same time, such information is fundamental in the advanced understanding of metal cycling in the environment.

2. Materials and methods

2.1. Collection and characterization of the tailings samples

105 The study area, known as Shimokawa mine, is located in the north-east part of Hokkaido, Japan
106 (Fig. 1). The tailings were produced from mining processes of gold (Au), silver (Ag), Cu, cobalt (Co),
107 Zn, and iron sulfide. The details were described by Khoeurn et al. (2018). The tailings samples were
108 collected at the depth of 1-3 meters because the samples were not weathered and contained higher
109 amounts of Cu, Zn, and Fe. The tailings samples were then air-dried, crushed using a mortar, and
110 sieved through a 2 mm aperture screen. A particle size of less than 2 mm was chosen for sequential
111 extraction, batch leaching and column experiments based on Japanese Standard Leaching Test. The
112 samples were then stored in air-tight containers to minimize exposure to moisture.
113 For chemical and mineralogical analyses, the samples were finely ground (< 75 μm) enhancing
114 uniformity of the sample. The chemical composition of the tailings was analyzed by using an X-ray
115 fluorescence spectrometer (XRF) (Spectro Xepos, Rigaku Corporation, Japan) while the mineralogical
116 composition was analyzed by using X-ray diffractometer (XRD) (MultiFlex, Rigaku Corporation,
117 Japan). The tailings samples were also observed by a high magnification optical microscope
118 (VHX-1000, Keyence Corporation, Japan) and then analyzed by scanning electron microscopy with
119 energy dispersive X-ray spectroscopy (SEM-EDX, SSX-550, Shimadzu Corporation, Japan).

120 *2.2. Sequential extraction*

121 Several different sequential extraction methods have been used to evaluate the mobility of Cu, Zn,
122 and Fe for contaminated soils, sediments, and mine wastes by a variety of authors (Tessier et al., 1979;
123 Dang et al., 2002; Marumo et al., 2003; Anju and Banerjee, 2010). The sequential extraction procedure
124 used in this study was based on Marumo et al. (2003) for the determination of the leachability of
125 hazardous metals from soils and sediments. Marumo et al. (2003) developed their method by revising
126 the procedure of Tessier et al. (1979) and Clevenger (1990). This method was applied to the tailings
127 sample (Clevenger, 1990; Dang et al., 2002; Anju and Banerjee, 2010). The details of the sequential
128 extraction procedure used in this study are summarized in Table 1. For the procedure, 1 g of the < 2
129 mm tailings sample was mixed with extractant. After the supernatant and residue were separated, the
130 residue of each extraction step was washed with 10 - 15 mL of deionized water. Then, the supernatant
131 and washing water were then combined in a 50 mL volumetric flask and diluted to 50 mL for analysis
132 by ICP-AES.

133 *2.3. Laboratory column experiments*

134 *2.3.1. Column set-up*

135 A column experiment is a kind of kinetic test that is commonly used to evaluate the long-term
136 geochemical behavior of mine wastes and soils. The experiment attempts to mimic natural weathering

of mine wastes in a laboratory scale. Thus, the experiment can provide information on sulfide oxidation rates and weathering characteristics of wastes (Benzaazoua et al., 2003), and is used to provide an indication of the change of the water quality in the drainage. A schematic diagram and details of the column dimensions are shown in Fig. S1. Three columns (cases 1, 2, and 3) were constructed and placed at room temperature. The columns are made of polyvinyl chloride (PVC) tubes mounted on the top of a steel stand accommodating three columns. The columns have a height of 300 mm and an inner diameter of 52 mm. Moreover, covers with small holes were also designed to simulate rainfall and protect the column from outside contaminants and dust. The columns were packed with 438 g of the tailings to a thickness of 15 cm for a bulk density of 1.374 g/cm^3 and porosity equal to 45 % (American Society for Testing and Materials, 1989).

2.3.2. *Irrigation and sample collection*

Distilled water (100, 200 and 400 cm^3), pH around 6, was introduced into the columns (cases 1, 2, and 3, respectively) once a week and allowed to flow down by gravity. Addition of distilled water started simultaneously for all columns until 84 weeks. After 2 days, the effluents were first collected for cases 2 and 3 while that of case 1 was first collected after the second rainfall introduction, meaning the second week of the experiment. Afterward, the effluents were collected 2 days after the irrigation. Spike tests with 1000 mg-Cu/L and 1000 mg-Zn/L were also conducted once in columns of cases 1 and 2 at week 37.

Immediately after collection of the effluents, the pH, oxidation-reduction potential (Eh), electrical conductivity (EC) and temperature were measured by pH meter (HORIBA F-71 pH meter, Japan), portable ORP meter (RM-30P, DKK-TOA corporation, Japan), and conductivity meter (HORIBA DS-12 conductivity meter, Japan), respectively. After that, the effluents were then filtered through a 0.45 μm Millex® filter and stored at room temperature prior to chemical analyses. The room temperature during the experimental period (March 2016–October 2017) was 20 ± 3 °C. The leaching of Cu, Zn, and Fe was not significantly affected by the variation of temperature.

2.3.3. Post-experiment characterization

After 84 weeks, the experiments were stopped because the leaching concentrations appeared to reach steady state. The tailings samples of each case were divided into sections 30 mm thick and air-dried for a few weeks. Chemical and mineralogical composition analyses and sequential extraction tests were conducted for the sectioned tailings using the same procedure mentioned earlier. Batch leaching tests were conducted to characterize the vertical profiles of leaching concentrations of Cu, Zn, and Fe. Fifteen grams of samples were mixed with 150 mL of deionized water (18 MΩ·cm) in a 250

mL Erlenmeyer flask and the suspensions were mixed using a lateral-reciprocating shaker at a speed of 200 rpm for 6 h at room temperature. After shaking, pH, Eh, EC, and temperature of the suspensions were measured, followed by filtration of the leachates with 0.45 μm Millex® filters (Merck Millipore, USA). All filtrates were preserved by adding hydrochloric acid (HCl) (pH < 2) prior to chemical analysis.

2.3.4. Chemical analysis

The concentrations of Cu, Zn, Fe, and coexisting ions in effluents and leachates were measured by inductively coupled plasma atomic emission spectrometer (ICP-AES) (ICPE-9000, Shimadzu Corporation, Japan), which was linearly calibrated from 0 to 10 mg/L with custom multi-element standard solution IV (1000 mg/L: Ag, Al, Ca, Cu, Fe, K, Mg, Mn, Na, and Zn) before running samples to be analyzed. Diluted solutions were also prepared using deionized water (18 MΩ·cm). The accuracy and precision of the analysis were tested through triplicate analyses of selected samples. Samples were diluted several times if needed. The results of the analyses using the standard method of ICP-AES had a margin of error of ca. 2–3 %, and the detection limits of these metals ranged from 0.001 to 0.01 mg/L, depending on element. Moreover, sulfur in the effluents and leachates was predominantly in the form of SO_4^{2-} based on the results of anion chromatograph (ICS-90, Dionex Corporation, USA), so for faster and easier determination of SO_4^{2-}, ICP-AES was used. For method of anion chromatograph, Dionex IonPak AS12A and AERS500 were used for the column and suppressor, respectively. The mixed solution of 2.7 mM Na_2CO_3 and 0.3 mM $NaHCO_3$ was applied for eluent. All chemicals used in the preparation and analysis were reagent grade.

2.4. Geochemical Modeling

To aid interpretation of the data, saturation indices (*SI*) of important minerals (i.e., oxyhydroxides, oxides, carbonates, and sulfates) that could potentially affect mobilities of metals were calculated using an equilibrium geochemical modeling software called PHREEQC (version 3.2.0-9820) (Parkhurst and Appelo, 1999) using the MINTEQ.V4.DAT database. This program is one of the most extensively used geochemical models.

3. Results

3.1 Characterization of tailings samples of the pre- and post-column experiments

The chemical compositions and mineralogical properties of the tailings samples of pre- and post-column experiments are shown in Table 2 and Fig. S2, respectively. Prior to the experiment, the

original tailings contained 43.3 wt% of SiO_2 and 9.08 wt% of Al_2O_3. The Si and Al indicate the presence of silicates and alumino-silicates in the gangue minerals. The tailings also contained 1.3 wt% of CaO, 0.1 wt% of MnO, and 3.8 wt% of MgO. It was highly enriched in Cu of 3,730 mg/kg and Zn of 17,500 mg/kg, respectively. The high contents of S and Fe_2O_3 were also found in the tailings of 11.2 wt% and 26.9 wt%, respectively. The tailings had a similar composition to other tailings reported elsewhere, in that they had higher amounts of Cu, Zn, Fe, and S (e.g., Gleisner and Herbert, 2002; Zhang et al., 2016; Christou et al., 2017).

After finishing column experiments, the contents of Cu, Zn, and S in the tailings were depleted, but Fe_2O_3 were similar for all cases (Table 2). The contents of Cu, Zn, and S were lower in the top tailings than those in the deeper tailings. Overall, the total contents of Cu, Zn, and S in case 1 were higher than those of cases 2 and 3 (case1 > case 2 > case 3) (Table 3). These differences may be due to the influence of the irrigation rate.

The mineralogy of the pre- and post-experiment is depicted in Fig. S2. The pre-experiment tailings were composed predominantly of quartz, chlorite, gypsum, anorthite, and pyrite while the post-experiment tailings similarly contained quartz, clinochlore, anorthite, and pyrite. Gypsum, however, was not detected in the post-experiment tailings. Although high contents of Cu and Zn in both the pre- and post-experiment tailings were observed, Cu and Zn-bearing minerals such as chalcopyrite and sphalerite were not detected by XRD. Carbonate minerals like calcite were not detected by XRD.

SEM-EDX investigation was performed for both pre- and post-experiment tailings samples (Figs. S3–S6). Samples from different depths were not shown here because the results were not dependent on depth. The SEM-EDX observation of the pre-experiment tailings showed the presence of silicate (SiO_2), S, Fe, Cu, and Zn (Fig. S3). However, it can be seen from the elemental mapping images that Cu, Zn, and Fe were presented in some areas of the tailings (a fine grain of Cu, Zn, and Fe; a large spot with high intensities of S and Si). These elements were also found in some parts of the post-experiment tailings samples of all cases (Figs. S4-S6). These results indicate that residual Cu, Zn, and Fe, and precipitated Fe still existed in the columns. The Si was likely related to quartz and chlorite/clinochlore while S was related to sulfide and sulfate minerals. This means that Cu, Zn, and Fe are likely associated with metal sulfides, such as chalcopyrite, sphalerite, and pyrite/iron oxyhydroxide/ferrihydrite, respectively, because pyrite was frequently observed in all samples.

3.2 Column experiments

The evolution of Cu, Zn, Fe, and major ions (Ca, Mg, K, SO_4^{2-}), as well as parameters involved in the oxidation-neutralization processes (pH, Eh, EC, Al, Mn, and Si) in the effluent of the columns, was observed. Figures 2, 3, and 4 represent the evolution of the measured data versus time. The plotted

values corresponded to the concentration released without considering the recovered volume of effluent or the mass of the solid sample.

3.2.1 pH, Eh, and EC of leachates

The changes in pH, Eh, and EC values of the effluents from the column experiments are illustrated in Figs. 2(a)-(c), respectively. The pH values in cases 1 (2.7–3.3, mean 3.1), 2 (2.5–3.4, mean 3.4), and 3 (2.7–3.7, mean 3.5) were observed. These pH values were in acidic condition throughout the experiments (84 weeks). At the beginning of the experiments, the pH values were lower in all cases and followed the order of case 3 > case 2 > case 1, and then they slightly increased and followed the order of case 3 ≈ case 2 > case 1 (Fig. 2 (a)). The oxic conditions were observed throughout the experiments (Fig. 2(b)). The Eh values in all three cases were variable (500-800 mV), but remained under oxidizing conditions throughout the duration of the experiments. This condition is favorable to the oxidation of residual sulfide minerals. The EC values of the effluents, which represent major ions present in the solution, were also monitored throughout the duration of the experiments. Figure 2(c) illustrates the evolution of EC in cases 1, 2, and 3. The highest EC values were found in the first leachate in all cases (28, 30, and 16 mS/cm for cases 1, 2, and 3, respectively) and decreased gradually as time elapsed. This implies that easily dissolved chemical species were released promptly after the addition of distilled water. The EC values were in the order of case 1 > case 2 > case 3. Lower pH values corresponded to higher EC values.

3.2.2 Leaching concentrations of Cu, Zn, Fe, and major ions

The leaching concentrations of Cu, Zn, and Fe in the effluents were higher at the beginning of the experiment, and then decreased dramatically within 10 weeks (Fig. 3). After that, the concentration fluctuated in lower concentration ranges. The leaching concentration ranges of Cu, Zn, and Fe were 0.1-1,950 mg/L, 4-22,100 mg/L, and 22-5,440 mg/L, respectively.

The changes in the concentrations of SO_4^{2-}, Al, Ca, K, Mg, Mn, and Si are illustrated in Figs. 3 and 4. As a general trend, the higher concentrations of these elements were observed at the beginning of the experiments, and then decreased and approached almost constant concentrations as time elapsed except for Ca. The Ca concentrations in cases 1 and 2 were similar for the first few weeks of the experiment, and almost constant from the beginning to week 20. As time elapsed, the concentration of Ca gradually decreased. The Ca concentration in case 3 was almost constant during the first few weeks and then gradually decreased throughout the experiment (Fig. 4 (a)).

3.2.3 Sequential extraction of the pre- and post-experiment tailings

The fraction of hazardous metals by sequential extraction could provide detailed information about the origin, chemical forms, biological and physico-chemical availability, mobilization, and transport of metals. Each of the fractions extracted represents a different form and different mechanism of availability (Tiesser et al., 1979; Clevenger 1990; Dang et al., 2002; Anju and Banerjee 2010). The results of the sequential extraction of Cu, Zn, and Fe of pre- and post-experiment tailings are presented in Fig. 5. The sequential extraction scheme is designed to target the fractions as listed in Table 1.

Prior to the experiment, Cu and Zn fractions were dominated by ion exchangeable fraction of 470 and 4,270 mg/kg, sulfide fractions of 460 and 1,350 mg/kg, and the residual fraction of 460 and 420 mg/kg, respectively. The large amount of Fe was mainly associated with the residual fraction of 30,800 mg/kg. Additionally, the Fe fraction associated with ion exchangeable, oxide, and sulfide fractions were 1,440, 19,100 and 11,700 mg/kg, respectively. In the post-experiment tailings, their exchangeable fractions (Case 1: Cu: 30-109 mg/kg, Zn: 20-50 mg/kg, and Fe: 90-190 mg/kg; Case 2: Cu: 40-90 mg/kg, Zn: 20-34 mg/kg, Fe: 80-110 mg/kg; Case 3: Cu: 20-92 mg/kg, Zn: 8-40 mg/kg, Fe: 80-120 mg/kg) were lower than the original. The sulfide fractions of Cu and Fe in the post-experiment tailings were almost the same as those in the pre-experiment tailings. However, the sulfide fraction of Zn in the post-experiment tailings was less than that in the pre-experiment tailings (Figs. 5 (b), (e), and (h)).

Overall, most of Cu, Zn, and Fe fractions in the original tailings were dominated by ion exchangeable, sulfide, and residual fractions while those in the post-experiment tailings were dominated by sulfide and residual fractions.

3.3 Vertical profiles of Cu, Zn, Fe, and SO_4^{2-} leaching after column experiments

Figure 6 shows the vertical profiles of Cu, Zn, Fe, and SO_4^{2-} leaching concentrations after column experiments. The lower pH values and leaching concentrations were found at the top tailings, and in overall the leaching concentration followed the order of case 1 > case 2 > case 3. However, the fact that the higher concentrations of Cu, Zn, Fe, and SO_4^{2-} were found in the deeper tailings sample agreed with the results of the field observation by Khoeurn et al. (2018). These results indicate that the exchangeable phase was almost flushed out from the top tailings (Fig. 5). This result might be a good indicative factor to reveal that oxidation prevails from the top tailings and less oxidation in the deeper tailings. The SO_4^{2-} concentrations were not significantly different with depth.

3.4 Spike tests of cases 1 and 2

The changes in Cu and Zn concentrations after spike tests for cases 1 and 2 are shown in Fig. 7. After adding the 1000 mg-Cu-Zn/L solution into columns at week 37, the peak concentrations of Cu and Zn appeared at week 39 in case 1 while their peaks were observed at week 38 in case 2. This means

that the leaching concentrations suddenly increased to their highest peaks (case 1: 70 mg/L of Cu; 380 mg/L of Zn at week 39 and case 2: 180 mg/L of Cu; 500 mg/L of Zn at week 38) were observed. Then, the concentration of Zn decreased to almost equal to the baseline concentration (case 1: 35 mg/L of Zn and case 2: 6 mg/L of Zn) before the spike tests, at week 45. Unlike the behavior of Zn, Cu concentration slowly decreased but was far higher than the baseline concentration (case 1: 3 mg/L of Cu and case 2: 7 mg/L of Cu) before the spike test. The recovery ratios of Cu were 38.9 and 48.3 % in cases 1 and 2, respectively, while those of Zn were 87.3 and 95.8 % in cases 1 and 2, respectively, by considering their baseline concentrations.

3.5 Geochemical calculation of effluents from column experiments

The results of *SI* calculations for the effluents from all cases throughout the experiments are presented in Fig. S7. The calculated *SIs* of chalcanthite, melanterite, goslarite, and kaolinite were strongly negative for all cases, implying dissolved (Fig. S7; Left). Those of cupricferite, goethite, lepidocrocite, maghemite, and K-jarosite were strongly positive, implying precipitated (Fig. S7; Right). Unlikely, *SI* values of ferrihydrite were distributed around zero, implying dissolution/precipitation equilibrium during the experiment, whereas that of gypsum was almost zero (almost saturated) at the beginning of the experiments for all cases and then decreased to less than zero with time (Fig. S7; Left). *SI* values of $AlOHSO_4$ and SiO_2 (am-gel) were around zero throughout the experiment, implying almost saturated (Fig. S7; Left).

4. Discussion

4.1 Effects of infiltration rate on the mobility of heavy metals and their leaching behaviors

In case 1 (the lowest infiltration rate), the first effluent sample of 66 mL was collected at the second week, whereas the effluent samples of 78 mL and 280 mL of cases 2 and 3 were collected at the first week, respectively. These results indicate that variations of the infiltration rate directly influenced the water residence time in the columns. Table 3 shows the water balance in all columns until 84 weeks of the experiment. The highest percentage of recovery was obtained in case 3 at 97.6%, followed by case 2 at 96% and case 1 at 93%. The differences between the volume of water added and collected are attributed to evaporation and residual water inside columns.

Overall, the pH value were in order of Case 3 > Case 2 > Case 1 while the Eh and EC values were in order of Case 1 > Case 2 > Case 3. Similar behaviors to EC were also observed for Cu, Zn, Fe, and major ions concentrations (Figs. 2-4). These results reveal that the infiltration rate plays a role as a dilution factor in these column experiments and also promotes mineral precipitation faster (high

intensity of Fe, O, S, and Si by SEM in Figs. S5 and S6). This is also supported by a reddish-brown color at the top tailings, which occurred more in case 3 followed by cases 2 and 1 after finishing the experiment (Fig. 10 (b)). The results of bulk chemical compositions showed that the highest depletion of Cu, Fe, Zn, and S were observed with the highest infiltration rate (Table 2).

4.2 Leaching concentration changes compared with fractions of metals by sequential extraction

Results from column experiments revealed that there were two patterns of leaching concentration of hazardous metals and ions. The first pattern is likely to be the dissolution of pre-existing soluble salts (i.e., gypsum), present in the sample prior to sample collection or oxidation products formed during sample storage. This is expected to influence chemistry of the effluent during the first few weeks of the experiment. The rapid dissolution of the soluble salts and hydrolysis of dissolved ions like Al^{3+}, Mg^{2+}, and Mn^{2+} were reported to occur during the onset of the wet season especially in the initial flushing event (Keith et al., 2001; Romero et al., 2007; Khorasanipour et al., 2011). The second pattern is a slow oxidation process of the remaining sulfide minerals due to the weathering process, which well agrees with Younger et al. (2002). The results of chemical, mineralogical, and geochemical calculations suggest that the effluent patterns in Figs. 3 and 4 were governed not only by oxidation of sulfide minerals, but also by the formation and dissolution of secondary phases and the sorption and co-precipitation of Cu and Zn to these phases.

Figures 8 ((a)-(c)) show the comparison between the cumulative release of Cu, Zn, and Fe from columns and fractions of Cu, Zn, and Fe by sequential extraction. The cumulative release of S is also shown in Fig. 8 (d). From the week 1 to 5 of column experiments, the cumulative releases of Cu, Zn, and Fe likely corresponded to ion exchangeable fraction. After week 5 of the experiments, the total leached amount of Cu is considered to be from the sulfide fraction of the sequential extraction, whereas that of Fe is likely from Fe-Mn oxides fraction. Zinc was completely leached out from the sulfide phase and continued to leach out from the residual fraction. This might be due to the remaining sulfide fraction in the residue fraction. The sequential extraction results revealed that the hazardous metals in the most mobile fraction (i.e., ion-exchangeable, carbonates, Mn-Fe oxides, and sulfides/organic matter) were the primary sources in the tailings. The ion exchangeable fraction is the most labile bonded to the tailings, and therefore, the most dangerous and bio-available for the environment. It consists of exchangeable fraction and soluble fraction in water under slightly acidic conditions. In the Fe-Mn oxide fraction, the metals are adsorbed or co-precipitated and are unstable under reduced conditions. In the sulfide/organic fraction, the metals are complexed and sorbed. Under oxidizing conditions, this fraction can be degraded to result in the release of soluble metals (Dang et al., 2002; Dold and Fonboté 2003). It can be assumed from this result that Cu, Zn, and Fe may continue to leach

out into the environment for a longer period of time by changing the fraction of dominant sources. In addition, the sample taken from the Shimokawa tailings contained higher contents of hazardous metals and S than those of the other tailings samples studied by many authors (Jurjovec et al., 2002; Ardau et al., 2009; Goumih et al., 2013; Zhang et al., 2016; Kandji et al., 2017). This means that the long-term leaching behavior of hazardous metals should be taken into account.

The cumulative releasing trends of Cu, Zn, Fe, and S from all columns during the experiment were nearly linear except for the first week of the experiment (previously stated that it was due to soluble salts). The cumulative release was in order of Zn > Cu > S > Fe. This implies that Zn is leached from the tailings at a higher rate than that of Cu. This result agreed with that of the spike tests (Fig. 7), which showed that Zn leaching was faster than Cu leaching.

4.3 Effects of Al and Si concentrations on pH changes in the effluents

Figures 9 ((a)-(c)) show concentrations of Al and Si in the effluents as a function of pH and the comparison between oxidation-neutralization curves for all cases, respectively. In case 1 (Fig. 9 (a)), the pH value was lower than those of cases 2 and 3, resulting in higher Al and Si concentrations in case 1 than those in cases 2 and 3 (Fig. 9 (b)-(c)). The Al and Si concentrations were negatively correlated with pH. This indicates that the oxidation of sulfide minerals resulted in the release of acid into the effluents of the tailings whereas gangue minerals such as alumino-silicate minerals incorporated in the tailings neutralized the acid. Their dissolution typically leads to a distinct sequence of pH buffering plateaus (Jurjovec et al., 2002). Gangue minerals contributing to acid-neutralization in the Shimokawa tailings are predominantly alumino-silicates. Consequent dissolution of alumino-silicate minerals within the sulfide oxidation zone also contributes to Al dissolution (Blowes et al., 1991; Jurjovec et al., 2002; Gunsinger et al., 2006).

Figure 9 (d) shows the oxidation-neutralization curves between cumulative molar concentrations of Al and Si and that of SO_4^{2-} based on the results of column experiments. The curves compared the evolution of the products of sulfide oxidation (dissolved S as sulfates in the experiments) with those of acid neutralization (Al and Si, which might be from alumino-silicate like anorthite). The curve of all cases shows two phases separated by an inflection point: a lower slope value in the early 15 weeks of the experiments followed by a steeper slope for the rest of the duration of the experiment. The steeper slope toward the neutralization products means that alumino-silicate (anorthite) and chlorite likely neutralize the AMD in the tailings. Although silicate dissolution rates increase under highly acidic conditions, corresponding pH buffering is generally minimal due to the relatively high rates of acid production (Jambor et al., 2002; Jurjovec et al., 2002; Salmon and Malsmström, 2006). In addition, the neutralizing capacity of some alumino-silicate is controversial since the Al released can generate

acidity after hydrolysis and precipitate as hydroxides (Kwong and Ferguson, 1997; Lappako and White, 2000).

4.4 Factors affecting pyrite oxidation

In the column experiments, oxidation of pyrite occurs by contacting with atmospheric, dissolved O_2 (DO), water, and/or microorganisms (Silverman, 1967). Theoretically, oxidation of 1 mole of pyrite consumes 3.5 moles of DO in order to produce 1 mole of Fe^{2+} and 2 moles of SO_4^{2-}. At 20 °C, the distilled water contained about 8.84 mgO_2/L (Langmuir, 1997). Based on Langmuir (1997), the DO of distilled water can be calculated. The calculation of DO consumed and Fe^{2+} and SO_4^{2-} produced after 6 weeks of experiments are shown in Table 4 by considering DO in the infiltration rate (distilled water) each week. The amount of DO consumed was far lower than those of Fe^{2+} and SO_4^{2-} produced, which means that oxidation of pyrite was not only affected by DO but also other factors, such as atmospheric O_2 and/or ferric iron (Fe^{3+}). At atmospheric exposure, pyrite oxidation begins within minutes, commencing with oxidation of S^{2-} species and producing SO_4^{2-} while iron-sulfate was produced within a few minutes (Chandra and Gerson, 2010). Sulfate is the main oxidation product of prolonged atmospheric exposure (Chandra and Gerson, 2010) and Todd et al. (2003) identified this to be largely presented as Fe-sulfate ($Fe_2(SO_4)_3$). The $Fe_2(SO_4)_3$ easily dissolves into Fe^{3+} and SO_4^{2-} when it contacts with water. The ferric iron (Fe^{3+}) is more aggressive and effective than O_2 for pyrite oxidation (Moses et al., 1987; Chandra and Gerson, 2010). Hence, there is markedly less direct oxidation potential in the deeper tailings of the column when compared with sub-aerial tailings (surface tailings).

Another support of oxidation occurring in the tailings is the difference of pre- and post-experiment S masses, which showed that considerable amounts of S were leached (Table 2). Sulfur was lost from all three columns in proportion to the irrigation rate. The overall decline in S over the course of the experiment is indicative of an ongoing process of oxidation. The concentration of Zn, Cu, Fe, and SO_4^{2-} still remained higher in the deeper tailings, which could support the continuous oxidation reduced with depth (Fig. 6) (Khoeurn et al., 2018).

4.5 Formation and dissolution of secondary minerals in the tailings during the column experiments

Figure 10 (a) shows the relationship between a total of molar concentrations of Ca, Mg, Cu, Mg, Zn, and Fe in the effluents and that of SO_4^{2-}. A green straight line in this figure shows the theoretical relationship by assuming stoichiometric dissolution of soluble salts (Eq. (1)-(4)). A red straight line shows the theoretical relationship by assuming stoichiometric dissolution of gypsum, pyrite, sphalerite, and chalcopyrite (Eq. (5)-(8)).

$$FeSO_4 \leftrightarrow Fe^{2+} + SO_4^{2-} \quad (1)$$

$$CuSO_4 \leftrightarrow Cu^{2+} + SO_4^{2-} \quad (2)$$

$$ZnSO_4 \leftrightarrow Zn^{2+} + SO_4^{2-} \quad (3)$$

$$MgSO_4 \leftrightarrow Mg^{2+} + SO_4^{2-} \quad (4)$$

Gypsum: $CaSO_4 .2H_2O \rightarrow Ca^{2+} + SO_4^{2-} + 2H_2O$ (5)

Pyrite: $FeS_{2(s)} + 7/2O_2 + H_2O \rightarrow Fe^{2+} + 2SO_4^{2-} + 2\ H^+$ (6)

Chalcopyrite: $CuFeS_2 + 4\ O_2 \rightarrow Cu^{2+} + Fe^{2+} + 2SO_4^{2-}$ (7)

Sphalerite: $ZnS + 2O_2 \rightarrow Zn^{2+} + SO_4^{2-}$ (8)

During the first 5 weeks of the experiments, the plots were likely on the theoretical line of soluble salts. These results agreed with the first pattern of leaching, soluble salt dissolution. From week 6 to 30 of the experiments, the plots were likely on the theoretical line of dissolution of gypsum, chalcopyrite, sphalerite, and pyrite, which means that slower oxidation process controlled the leaching concentrations of Cu, Zn, Fe, and SO_4^{2-} in the effluents. As time elapsed, the slope of actual molar concentrations was lower than the theoretical line. Thus, at least two phenomena could explain this difference. The first is the precipitation of secondary minerals like iron-oxyhydroxide/ferrihydrite. The second is co-precipitation or adsorption of Cu and Zn onto the surface of these secondary minerals. The iron (III)-precipitates were clearly observed by the reddish-brown color of the tailings at the top of the column (Fig. 10 (b)). In addition, the calculation of *SI*s by PHREEQC also demonstrated that secondary minerals, such as ferrihydrite, goethite, maghemite, lepidocrocite, and cupricferite were precipitated in the system (Fig. S7). Another possible evidence for precipitation of secondary phases is that the SEM-EDS observations of samples after the experiment revealed the presence of iron-oxyhydroxide.

An Eh-pH diagram illustrating the speciation of Fe was also created with the measured pH and Eh values during the column experiments (Fig. 11). All of the plots in all cases were localized around the boundary of Fe^{2+}, $FeOH^{2+}$, and hematite. Hematite crystals can be formed as a secondary mineral by weathering processes in soil, and along with other iron oxides or oxyhydroxides such as goethite (Hammarstrom et al., 2005).

Ferrous iron (Fe^{2+}) might be oxidized to ferric iron (Fe^{3+}) (Eq. 9). At neutral or higher pH level, Fe^{3+} can precipitate (Eq. 10). But, at very low pH level, it can remain in solution and act as the electron acceptor in pyrite oxidation (Eq. 11) (Singer and Stumm, 1970).

$$Fe^{2+} + 1/4O_2 + H+ \rightarrow Fe^{3+} + 1/2\ H_2O \quad (9)$$

$$Fe^{3+} + 3\ H_2O \leftrightarrow Fe(OH)_{3(s)} + 3H^+ \quad (10)$$

$$FeS_{2(s)} + 14Fe^{3+} + 8H_2O \rightarrow 15Fe^{2+} + 2SO_4^{2-} + 16H^+ \quad (11)$$

The cycle of reactions (9)-(11) is likely to occur during the column experiments. The iron precipitates can act as a sink of trace elements (Cu, Pb, Se, and Zn) through adsorption and/or co-precipitation (Khorasanipour et al., 2011; McGregor and Blowes, 2002). This may contribute to the

458 decrease in Cu, Zn, and Fe concentrations in the effluents.

459 **5. Conclusion**

460 Chemical characterization of effluents from the tailings of a closed mine site was performed to
461 understand the leaching behaviors of hazardous metals (i.e., Cu, Zn, and Fe) from the tailings and to
462 compare with the results of the sequential extraction. The findings are the following:

463 1) Pyrite oxidation likely occurred by the exposure to atmospheric O_2 and contact with DO and
464 Fe^{3+}, which resulted in acidic pH in the effluents. Such an acidic pH could dissolve hazardous
465 metals, such as Cu and Zn as well as alumino-silicate and chlorite into the effluents. The
466 dissolution of alumino-silicate and chlorite could neutralize the pH for a longer period of the
467 experiments.

468 2) The main release mechanisms of Cu, Zn, and Fe were considered into three phases. At the first
469 and the second phases, they were released by the easy dissolution of more labile species (ion
470 exchangeable and sulfates) and oxidation of the remaining sulfide minerals (sulfide fraction) in the
471 tailings. At the third phase, their release mechanisms were still controlled by oxidation of the
472 remaining sulfide minerals but some of Fe was precipitated (Fe-Mn oxide fraction), such as iron
473 oxyhydroxides/ferrihydrite, maghemite, lepidocrocite, and goethite. These minerals could act as a
474 sink for Zn and Cu by co-precipitation or adsorption.

475 3) The releasing rate of hazardous metals was in the order of Zn > Cu > Fe and significant amounts
476 of Cu, Zn, Fe, and S existed in the columns at the end of the experiments. This suggests that
477 residual minerals continue to produce acidic water and hazardous metals.

478 4) The highest irrigated rainfall resulted in diluting the concentrations of hazardous metals in the
479 effluents as well as pH values and promoted faster precipitation of secondary minerals. Based on
480 these results, the irrigation rate is one of the important parameters that should be considered when
481 designing a remediation system.

482

483 **6. Acknowledgments**

484 The authors gratefully appreciate Eco Management Co., Ltd. for the assistance during the field
485 sampling and for providing us with the geological data of the study site.

486

References

Álvarez-Valero, A.M., Sáez, R., Pélez-López, R., Delgado, J., Nieto, J.M., 2009. Evaluation of heavy metal bio-availability from Almagrera pyrite-rich tailings dam (Iberian Pyrite Belt, SW Spain) based on a sequential extraction procedure. J. Geochem. Explor. 102, 87-94.

American Society for Testing and Materials, 1989. Standard test method for leaching solid waste in column apparatus (Method D 4874-89). American Society for Testing and Materials, Philadelphia, PA.

Anju, M., Banerjee, D.K., 2010. Comparison of two sequential extraction procedures for heavy metals partitioning in mine tailings. Chemophere, 78, 1393-1402.

Ardau, C., Blowes, D.W., Ptacek, C.J., 2009. Comparison of laboratory testing protocols to field observations of the weathering of sulfide-bearing mine tailings. J. Geochem. Explor. 100, 182-191.

Benzaazoua, M., Bussière, B., Dagenais, A.M., Archambault, M., 2003. Kinetic test comparison and interpretation for prediction of the Joutel tailings acid generation potential. Environ. Geol. 46, 1086-1101.

Blowes, D.W., Reardon, E.J., Jambor, J.L., Cherry, J.A., 1991. The formation and potential importance of cemented layers in inactive sulfide mine tailings. Geochim. Cosmochim. Acta 55, 965-978.

Buckby, T., Black, S., Coleman, M.L., Hodson, M.E., 2003. Fe-sulphate-rich evaporative mineral precipitates from the Rio Tinto, southwest Spain. Mineral. Mag. 67, 263–278.

Carbone, C., Dinelli, E., Marescotti, P., Gasparotto, G., Lucchetti, G., 2013. The role of AMD secondary minerals in controlling environmental pollution: Indications from bulk leaching tests. J. Geochem. Explor. 132, 188–200.

Chandra, A.P., Gerson , A.R., 2010. The mechanisms of pyrite oxidation and leaching: A fundamental perspective. Surf Sci Rep. 65, 293–315.

Cheong, Y.W., Ji, S.W., Ahn, J.S., Yim, G.J., Min, D.S., McDonald, L.M., 2012. Seasonal effects of rainwater infiltration on volumetric water content and water quality in mine wastes at the Gyopung mine, South Korea. J. Geochem. Explor. 116, 8-16.

Christou, A., Theologides, C.P., Costa, C., 2017. Assessment of toxic heavy metals concentrations in soils and wild and cultivated plant species in Limni abandoned copper mine site, Cyprus. J. Geochem. Explor. 178, 16-22.

Clevenger, T.E., 1990. Use of sequential extraction to evaluate the heavy metals in mining wastes. Water Air Soil Pollut. 50, 241-253.

Dang, Z., Liu, C., Haigh, M., 2002. Mobility of heavy metals associated with the natural weathering of coal mine spoils. Environ. Pollut. 118, 419-426.

Dold, B., 1999. Mineralogical and geochemical changes of copper flotation tailings in relation to their original composition and climatic setting–implications for acid mine drainage and element mobility. Terre Environ. 18, 1–230.

Dold, B., 2003. Speciation of the most soluble phases in a sequential extraction procedure adapted for geochemical studies of copper sulfide mine waste. J. Geochem. Explor. 80, 55–68.

Dold, B., Fontboté, L., 2001. Element cycling and secondary mineralogy in porphyry copper tailings as function of climate, primary mineralogy, and mineral processing. J. Geochem. Explor. 74, 2–55.

Flohr, M.J.K., Dillenber, R.G., Plumlee, G.S., 1995. Characterization of secondary minerals formed as

the result of weathering of the Anakeesta formation, great smoky mountains National Park, Tennessee. U.S. Geol. Survey Open-file. pp. 95–477.
Frau, F., 2000. The formation–dissolution–precipitation cycle of melanterite at the abandoned pyrite mine of Genna Luas in Sardinia, Italy–environmental implications. Mineral. Mag. 64, 995–1006.
Gleisner, M., Herbert, Jr., R.B., 2002. Sulfide mineral oxidation in freshly processed tailings: Batch experiments. J. Geochem. Explor. 76, 139-153.
Goumih, A., Adnani, M.E., Hakkou, R., Benzaazoua, M., 2013. Geochemical behavior of mine tailings and waste rock at the abandoned Cu-Mo-W azegour mine (Occidental High Atlas, Morocco). Mine Water Environ. 32, 121-132.
Gunsinger, M.R., Ptacek, C.J., Blowes, D.W., Jambor, J.L., Moncur, M.C., 2006. Mechanisms controlling acid neutralization and metal mobility within a Ni-rich tailings impoundment. Appl. Geochem. 21, 1301–1321.
Hammarstrom, J.M., Seal, R.R., Meier, A.L., Kornfeld, J.M., 2005. Secondary sulfate minerals associated with acid drainage in the eastern US: Recycling of metals and acidity in surficial environments. Chem. Geol. 215, 407–431.
Jambor, J., Dutrizac, J., Groat, L., Raudsepp, M., 2002. Static tests of neutralization potentials of silicate and aluminosilicate minerals. Environ. Geol. 43, 1–17.
Jurjovec, J., Ptacek, C.J., Blowes, D.W., 2002. Acid neutralization mechanisms and metal release in mine tailings: A laboratory column experiment. Geochim. Cosmochim. Acta 66, (9) 1511-1523.
Kandji, E.H.B., Plante, B., Bussiere, B., Beaudoin, G., 2017. Kinetic testing to evaluate the mineral carbonation and metal leaching potential of ultramafic tailings: Case study of the Dumont Nickel Project, Amos, Québec. Appl. Geochem. 84, 262-276.
Keith, D.C., Runnells, D.D., Esposito, K.J., Chermak, J.A., Levy, D.B., Hannula, S.R., Watts, M., Hall, L., 2001. Geochemical models of the impact of acidic groundwater and evaporative sulfate salts on Boulder Creek at Iron Mountain, California. Appl. Geochem. 16, 947–961.
Khoeurn, K., Sasaki, A., Tomiyama, S., Igarashi, T., 2018. Distribution of zinc, copper, and iron in the tailings dam of an abandoned mine in Shimokawa, Hokkaido, Japan. Mine Water Environ. https://doi.org/10.1007/s10230-018-0566-5 (in press)
Khorasanipour, M., Tangestani, M.H., Naseh, R., Hajmohammadi, H., 2011. Hydrochemistry, mineralogy and chemical fractionation of mine and processing wastes associated with porphyry copper mines: A case study from the Sarcheshmeh mine, SE Iran. Appl. Geochem. 26, 714–730.
Kwong, Y.T.J., Ferguson, K.D., 1997. Mineralogical changes during NP determinations and their implications. In: Proceedings of 4th international conference on acid rock drainage (ICARD), Vancouver, BC, Canada, pp 435-447.
Langmuir, D., 1997. Aqueous Environmental Geochemistry. Prentice Hall, Upper Saddle River.
Lappako, K.A., White, W.W., 2000. Modification of the ASTM 5744-96 kinetic test. Proceedings of 5th ICARD, Denver, CO, USA, Vol 1, pp. 631-639.
Lindsay, M.B.J., Moncur, M.C., Bain, J.G., Jambor, J.L., Ptacek, C.J., Blowes, D.W., 2015. Geochemical and mineralogical aspects of sulfide mine tailings. Appl. Geochem. 57, 157-177.
Marumo, K., Ebashi, T., Ujiie, T., 2003. Heavy metal concentration leacheabilities and lead isotope ratio of Japanese soils. Shigen - Chisitsu, 53 (2), 125-146 (in Japanese with English abstract).
McGregor, R.G., Blowes, D.W., 2002. The physical, chemical and mineralogical properties of three cemented layers within sulfide-bearing mine tailings. J. Geochem. Explor. 76, 195-207.
Modabberi, S., Alizadegan, A., Mirnejad, H., Esmaeilzadeh, E., 2013. Prediction of AMD generation potential in mining waste piles in the sarchesmeh porphyry copper deposit, Iran. Environ. Monit.

574 Assess. 185, 9077-9087.
575 Moncur, M.C., Jambor, J.L., Ptacek, C.J., Blowes, D.W., 2009. Mine drainage from the weathering of
576 sulfide minerals and magnetite. Appl. Geochem. 24, 2362‑2373.
577 Moses, C.O., Nordstrom, D.K., Herman, J.S., Mills, A.L., 1987. Aqueous pyrite oxidation by dissolved
578 oxygen and by ferric iron. Geochim. et Cosmochim. Acta 51, 1561-1571.
579 Nordstrom, D.K., 2011. Hydrogeochemical processes governing the origin, transport and fate of major
580 and trace elements from mine wastes and mineralized rock to surface waters. Appl. Geochem. 26,
581 1777–1791.
582 Olyphant, G.A., Bayless, G.R., Harper, D., 1991. Seasonal and weather-related controls on solute
583 concentrations and acid drainage from a pyritic coal-refuse deposit in southwestern Indiana USA.
584 J. Contam. Hydrol. 7, 219–236.
585 Paul, L.Y., Banwart, S.A., Hedin, R.S. (2002). Mine water, Hydrology, Pollution, Remediation. Environ.
586 Pollut. 5, 42-43.
587 Parkhurst, D.L., Appelo, C.A.J., 1999. User's Guide to PHREEQC (Version 2) - A computer program
588 for speciation, batch-reactions, one-dimensional transport, and reverse geochemical calculations.
589 Water-Resources Investigations Report 99-4259, U.S. Department of the interior and U.S
590 geological survey, Denver, CO.
591 Redwan, M., Rammlmair, D., 2012. Influence of climate, mineralogy and mineral processing on the
592 weathering behaviour within two, low-sulfide, high-carbonate, gold mine tailings in the Eastern
593 Desert of Egypt. Environ. Earth Sci. 65, 2179–2193.
594 Romero, F.M., Armienta, M.A., Gonzalez-Hernandez, G. 2007. Solid-phase control on the mobility of
595 potentially toxic elements in an abandoned lead/zinc mine tailings impoundment, Taxco, Mexico.
596 Appl. Geochem. 22, 109-127.
597 Root, R.A., Hayes, S.M., Hammond, C.M., Maier, R.M., Chorover, J., 2015. Toxic metal(loid)
598 speciation during weathering of iron sulfide mine tailings under semi-arid climate. Appl.
599 Geochem. 62, 131-149.
600 Salmon, S.U., Malmström, M.E., 2006. Quantification of mineral dissolution rates and applicability of
601 rate laws: Laboratory studies of mill tailings. Appl. Geochem. 21, 269–288.
602 Schuwirth, N., Voegelin, A., Kretzschmar, R., Hofmann, T., 2007. Vertical distribution and speciation
603 of trace metals in weathering flotation residues of a zinc/lead sulfide mine. J. Environ. Qual. 36,
604 61–69.
605 Shu, W.S., Ye, Z.H., Lan, C.Y., Zhang, Z.Q., Wong, M.H., 2001. Acidification of lead/zinc mine tailings
606 and its effect on heavy metal mobility. Environ. Int. 26, 389–394.
607 Silverman, M.P., 1967. Mechanism of bacterial pyrite oxidation. J. Bacteriol. 94, 1046-1051.
608 Singer, P.C., Stumm, W., 1970. Acid mine drainage–rate determining step. Science 167, 1121-1123.
609 Smuda, J., Dold, B., Friese, K., Morgenstern, P., Glaesser, W., 2007. Mineralogical and geochemical
610 study of element mobility at the sulfide-rich Excelsior waste rock dump from the polymetallic
611 Zn-Pb-(Ag-Bi-Cu) deposit, Cerro de Pasco, Peru. J. Geochem. Explor. 92, 97-110.
612 Tessier, A., Cambell, G.C., Bisson, M., 1979. Sequential extraction procedure for the speciation of
613 particulate trace metals. Anal. Chem. 51, 844-850.
614 Todd E.C., Sherman, D.M., Purton, J.A. 2003. Surface oxidation of chalcopyrite ($CuFeS_2$) under
615 ambient atmospheric and aqueous (pH 2-10) conditions: Cu, Fe L- and O K-edge X-ray
616 spectroscopy. Geochim. Cosmochim. Acta 67, 2137-2146.
617 Wang, L., Li, Y., Wang, H., Cui, X., Wang, X., Lu, A., Wang, X., Wang, C., Gan, D., 2017. Weathering
618 behavior and metal mobility of tailings under an extremely arid climate at Jinchuan Cu-Ni sulfide

deposit, Western China. J. Geochem. Explor. 173, 1-12.
Younger, P.L., Banwart, S.A., Hedin, R.S., 2002. Mine Water Hydrology, Pollution, Remediation. Kluwer Academic Publishers, London.
Yeheyis, M.B., Shang, J.Q., Yanful, E.K., 2009. Long-term evaluation of coal fly ash and mine tailings co-placement: A site-specific study. J. Environ. Manag. 91, 237-244.
Zhang, W., Alakangas, L., Wei, Z., Long, J., 2016. Geochemical evaluation of heavy metal migration in Pb-Zn tailings covered by different topsoils, J. Geocem. Explor. 165, 134-142.

Figure captions

Figure 1 (a) The map of study area, Shimokawa, Hokkaido, Japan, and (b) plain view of the tailings dam (Khoeurn et al., 2018)

Figure 2 Changes in pH (a), Eh (b), and EC (c) with time for column effluents

Figure 3 Changes in concentrations of (a) Cu, (b) Zn, (c) Fe, and (d) SO_4^{2-} with time for column effluents

Figure 4 Changes in concentrations of (a) Ca, (b) Al, (c) Mg, (d) Mn, (e) K, and (f) Si with time for column effluents

Figure 5 Sequential extraction of the pre- and post-experiment tailings in Case 1: (a) Cu, (b) Zn, and (c) Fe; Case 2: (d) Cu, (e) Zn, and (f) Fe ; and Case 3: (g) Cu, (h) Zn, and (i) Fe

Figure 6 Vertical profiles of pH, and Zn, Cu, Fe, and SO_4^{2-} concentrations of post-experiment tailings by batch leaching tests

Figure 7 Changes in concentrations of Cu and Zn for cases 1 and 2 during spike tests

Figure 8 Cumulative releasing of Cu, Zn, Fe, and S from the tailings of column experiments with time and sequential extraction

Figure 9 Concentrations of Al and Si versus pH from column experiments ((a), (b), and (c)); comparison between the oxidation-neutralization curves

Figure 10 (a) Relationship between observed concentrations in effluents from the columns and theorictical stoiciochemistry by considering pyrite, chalcopyrite, and sphalerite oxidation and gypsum dissolution (red line), and dissolution of soluble salts (green line) and (b) image of columns in cases 1, 2, and 3

Figure 11 Eh-pH predominance diagram of Fe at T = 25 °C, P = 1.013 bars, Fe activity = 10-9, H_2O activity = 1. The plots represent Eh and pH values of effluents from the columns in all cases.

Table 1 Details of sequential extraction procedure

Steps	Extractant	pH	Liquid to solid ratio (mL/g)	Temperature (°C)	Duration (h)	Mixing speed (rpm)	Extracted phase
1	1 M $MgCl_2$	7	20/1	25	1	200	Exchangeable
2	1 M CH_3COONa	5	20/1	25	5	200	Carbonates
3	0.04 M $NH_2OH.HCl$ in 25% acetic acid	5	20/1	50	5	200	Fe-Mn oxides
4	0.04 M $NH_2OH.HCl$ in 25% acetic acid; 30% H_2O_2; 0.02 M HNO_3	5	36/1	85	5	200	Sulfide/ organics mater
5			Calculated				Residual

Table 2 Mineralogical composition of the tailings before and after column experiments

Depth (cm)	SiO_2 wt%	TiO_2 wt%	Al_2O_3 wt%	Fe_2O_3 wt%	MnO wt%	MgO wt%	CaO wt%	Na_2O wt%	K_2O wt%	P_2O_5 wt%	S wt%	Cu mg/kg	Zn mg/kg	Pb mg/kg
Pre-tailings	43.30	0.41	9.08	26.85	0.10	3.77	1.32	< 0.1	0.61	0.13	11.24	3,730	17,480	48.7
Post-tailings: Case 1														
0-3	43.39	0.42	8.63	24.41	0.07	3.56	0.81	< 0.1	0.60	0.24	8.20	2,720	5,280	48.1
3-6	41.03	0.44	8.58	24.71	0.08	3.52	0.81	< 0.1	0.60	0.23	8.92	2,930	7,860	55.6
6-9	49.98	0.47	10.77	28.88	0.08	4.70	0.98	< 0.1	0.72	0.38	11.31	3,300	7,870	44.8
9-12	40.65	0.41	8.61	24.29	0.08	3.46	0.90	< 0.1	0.57	0.21	9.00	3,930	10,770	61.4
12-15	41.53	0.41	8.98	23.56	0.07	3.69	0.84	< 0.1	0.59	0.24	8.90	3,160	7,980	48.4
Post-tailings: Case 2														
0-3	41.29	0.43	8.76	25.54	0.08	3.53	0.73	< 0.1	0.60	0.25	8.50	2,880	4,920	47.8
3-6	41.05	0.38	8.67	23.39	0.07	3.57	0.69	< 0.1	0.54	0.24	9.06	2,590	4,660	48.5
6-9	42.34	0.38	9.59	22.78	0.07	3.90	0.76	< 0.1	0.56	0.26	8.68	3,150	7,020	49.8
9-12	42.92	0.40	9.62	22.95	0.08	3.90	0.84	< 0.1	0.59	0.19	8.23	3,680	8,950	57.9
12-15	50.83	0.48	10.96	28.08	0.09	4.70	1.07	< 0.1	0.72	0.30	10.53	4,070	11,390	69.4
Post-tailings: Case 3														
0-3	45.25	0.43	9.28	25.45	0.08	3.72	0.74	0.36	0.62	0.22	6.78	2,540	3,370	53
3-6	42.53	0.39	8.60	23.61	0.07	3.60	0.71	0.15	0.56	0.23	8.33	2,380	4,040	46.1
6-9	44.78	0.41	9.08	21.75	0.07	3.86	0.80	< 0.1	0.57	0.23	8.30	2,990	7,370	38.8
9-12	44.88	0.42	9.45	22.58	0.08	3.90	0.87	< 0.1	0.58	0.23	7.63	3,630	9,200	58.3
12-15	59.73	0.33	12.43	18.67	0.06	5.62	0.73	< 0.1	0.49	0.25	9.85	2,420	6,990	34.9

Table 3 Water balances in the columns throughout the experiments (84 weeks)

Cases	Total volume of influent (mL)	Total volume of effluent (mL)	Total volume retained and lost (mL)
1	8,400	7,785	615
2	16,800	16,167	633
3	33,600	32,804	796

Table 4 Mass balance of amount of consumed dissolved oxygen and produced Fe and SO_4^{2-} by pyrite oxidation

Cases	Dissolved oxygen (mole)	Iron (Fe^{2+}) (mole)	Sulfate (SO_4^{2-}) (mole)
1	$0.3\times10^{-4} \pm 0.015\times10^{-4}$	$2.7\times10^{-4} \pm 1.72\times10^{-4}$	$15.4\times10^{-4} \pm 2.8\times10^{-4}$
2	$0.55\times10^{-4} \pm 0.03\times10^{-4}$	$2.6\times10^{-4} \pm 1.1\times10^{-4}$	$9.7\times10^{-4} \pm 3\times10^{-4}$
3	$1.1\times10^{-4} \pm 0.06\times10^{-4}$	$4.4\times10^{-4} \pm 1.2\times10^{-4}$	$13.9\times10^{-4} \pm 3.3\times10^{-4}$

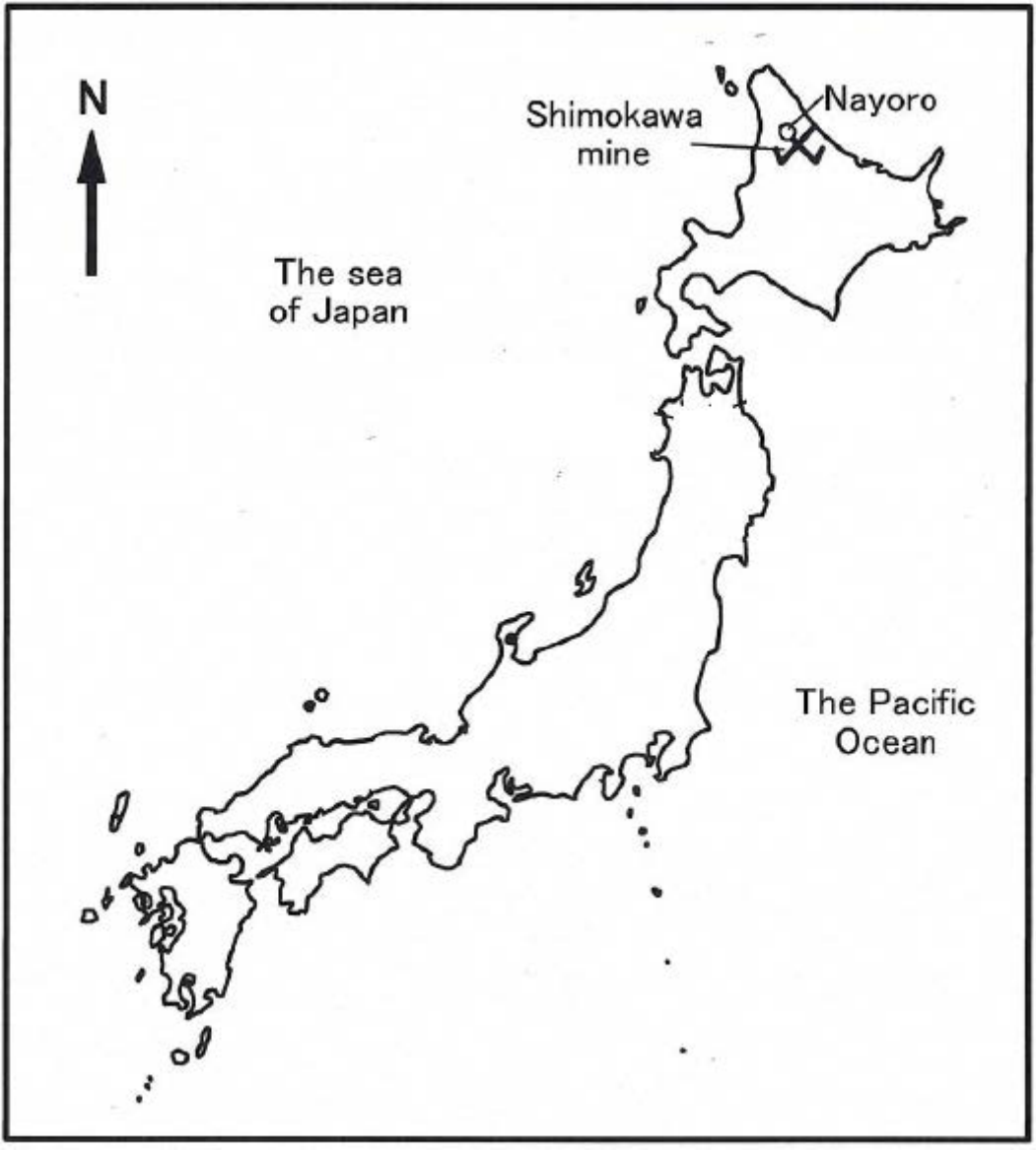
N
Shimokawa
mine
Nayoro
The sea
of Japan
The Pacific
Ocean

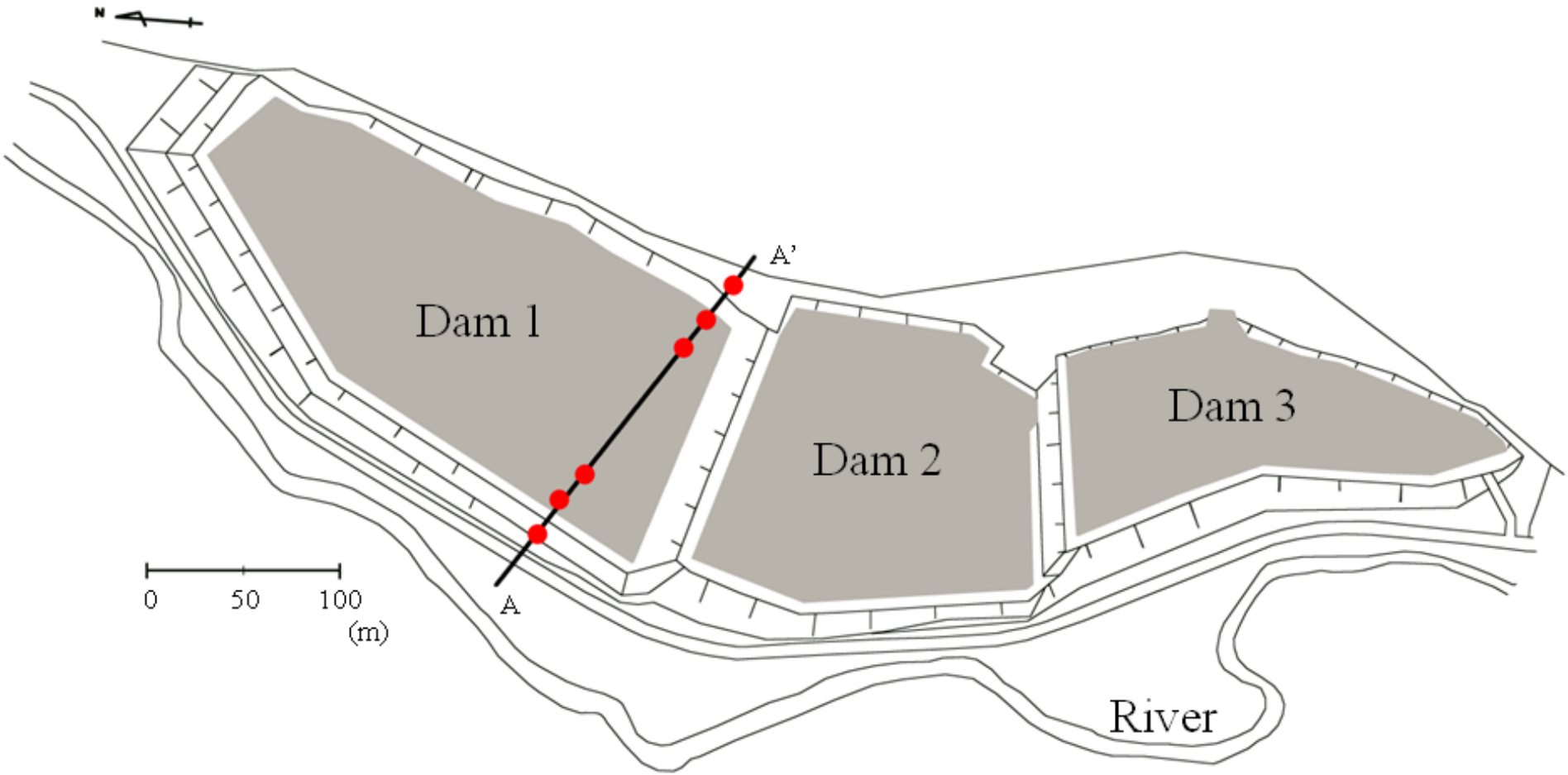
N
Dam 1
Dam 2
Dam 3
A'
A
0
50
100
(m)
River

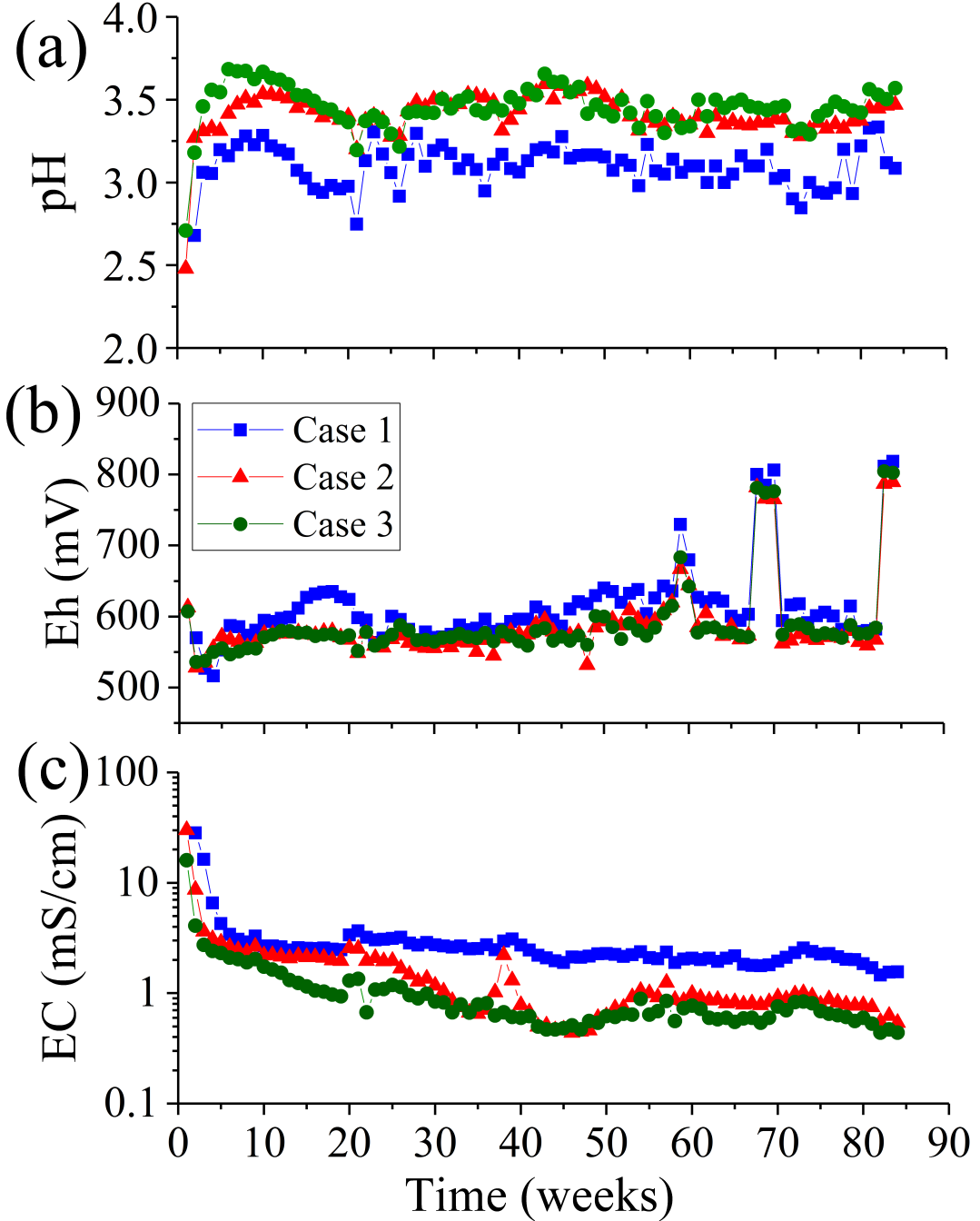
(a)
pH
4.0
3.5
3.0
2.5
2.0
(b)
Eh (mV)
900
800
700
600
500
Case 1
Case 2
Case 3
(c)
EC (mS/cm)
100
10
1
0.1
0
10
20
30
40
50
60
70
80
90
Time (weeks)

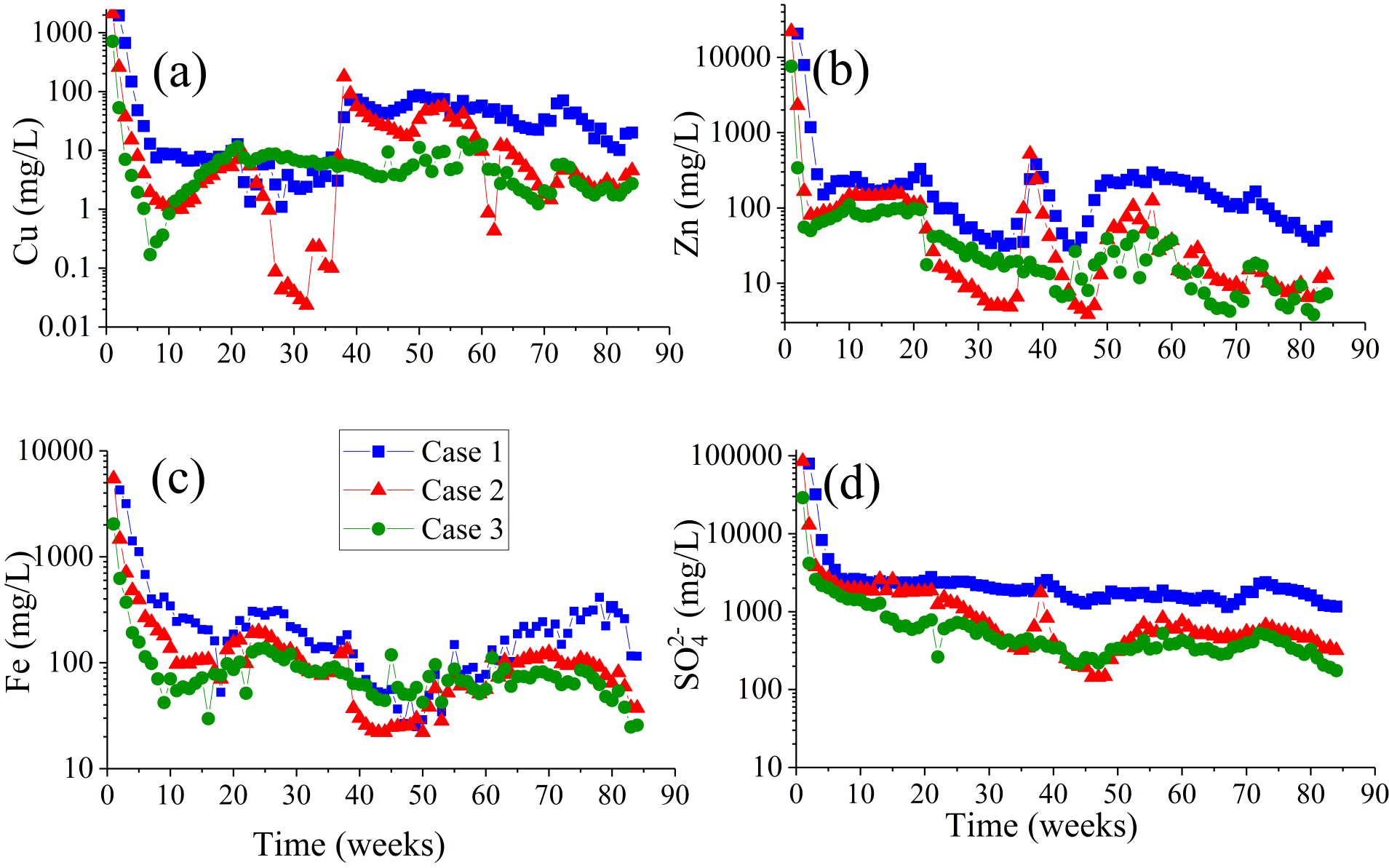
(a)
Cu (mg/L)
1000
100
10
1
0.1
0.01
0
10
20
30
40
50
60
70
80
90
(b)
Zn (mg/L)
10000
1000
100
10
(c)
Fe (mg/L)
Case 1
Case 2
Case 3
Time (weeks)
(d)
SO_4^{2-} (mg/L)
100000
Time (weeks)

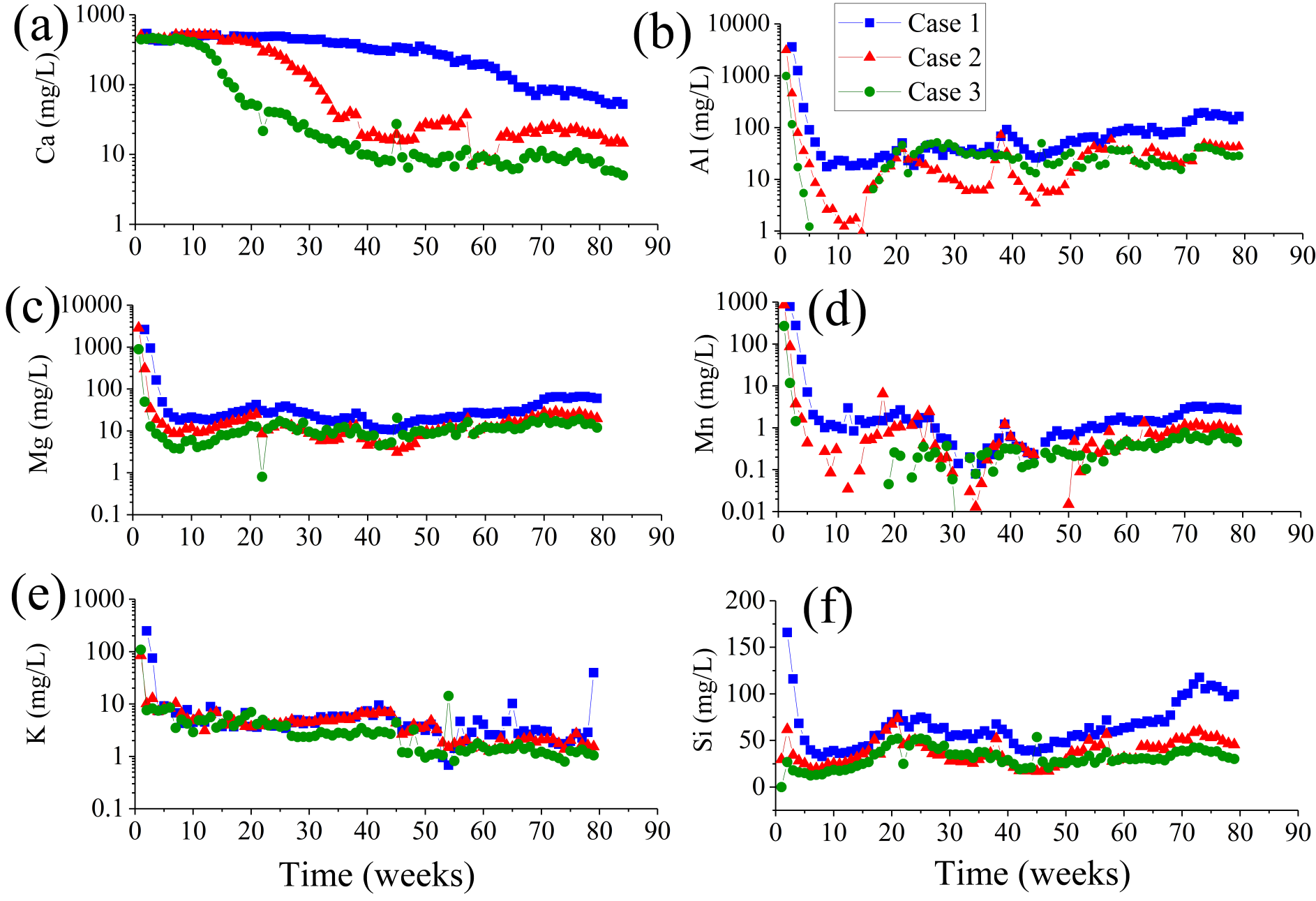
(a)
Ca (mg/L)
1000
100
10
1
0 10 20 30 40 50 60 70 80 90
(b)
Al (mg/L)
10000
1000
100
10
1
Case 1
Case 2
Case 3
(c)
Mg (mg/L)
10000
1000
100
10
1
0.1
(d)
Mn (mg/L)
1000
100
10
1
0.1
0.01
(e)
K (mg/L)
1000
100
10
1
0.1
Time (weeks)
(f)
Si (mg/L)
200
150
100
50
0
Time (weeks)

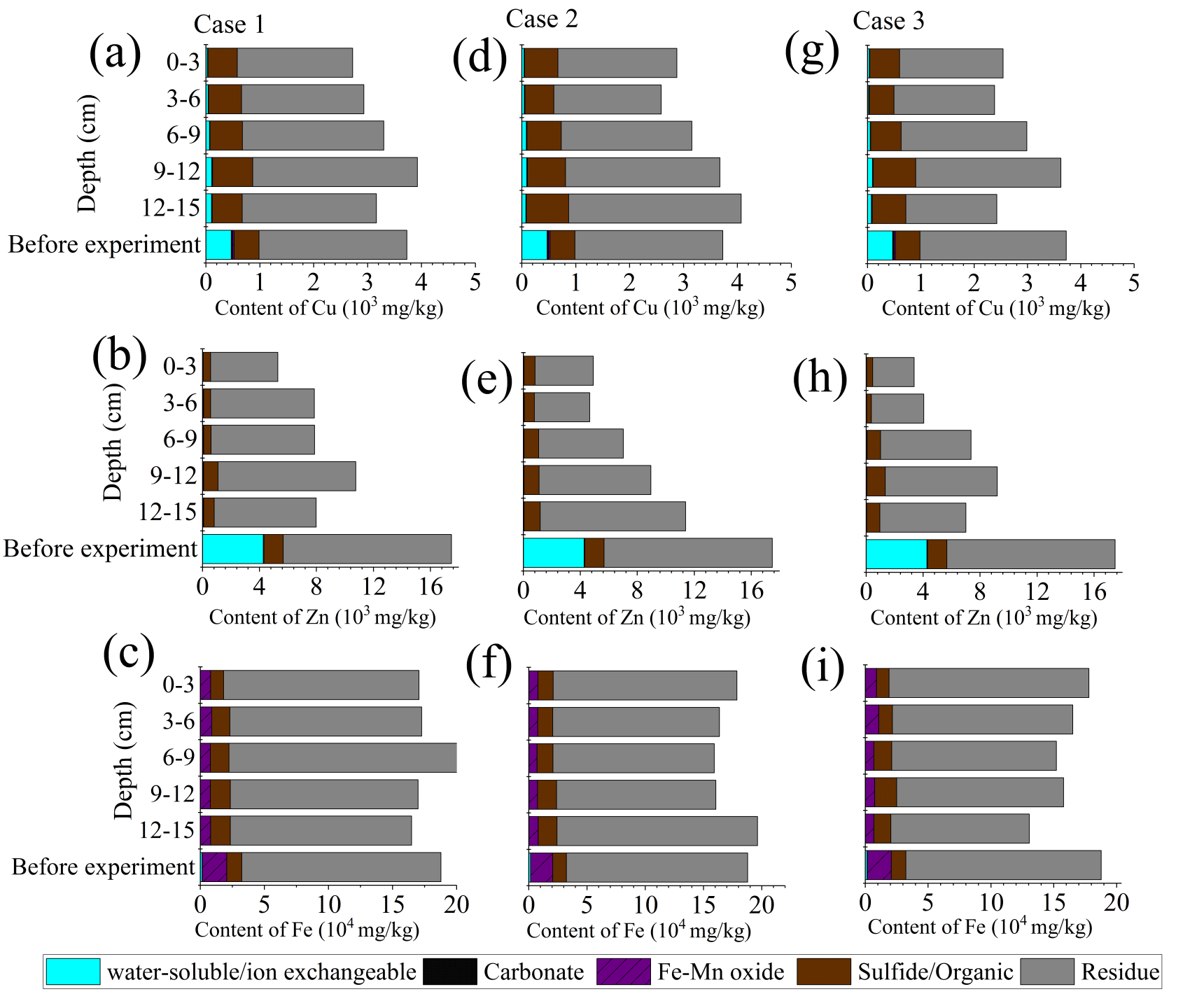
Case 1
Case 2
Case 3
(a)
(b)
(c)
(d)
(e)
(f)
(g)
(h)
(i)
Depth (cm)
0-3
3-6
6-9
9-12
12-15
Before experiment
Content of Cu (10^3 mg/kg)
Content of Zn (10^3 mg/kg)
Content of Fe (10^4 mg/kg)
water-soluble/ion exchangeable
Carbonate
Fe-Mn oxide
Sulfide/Organic
Residue

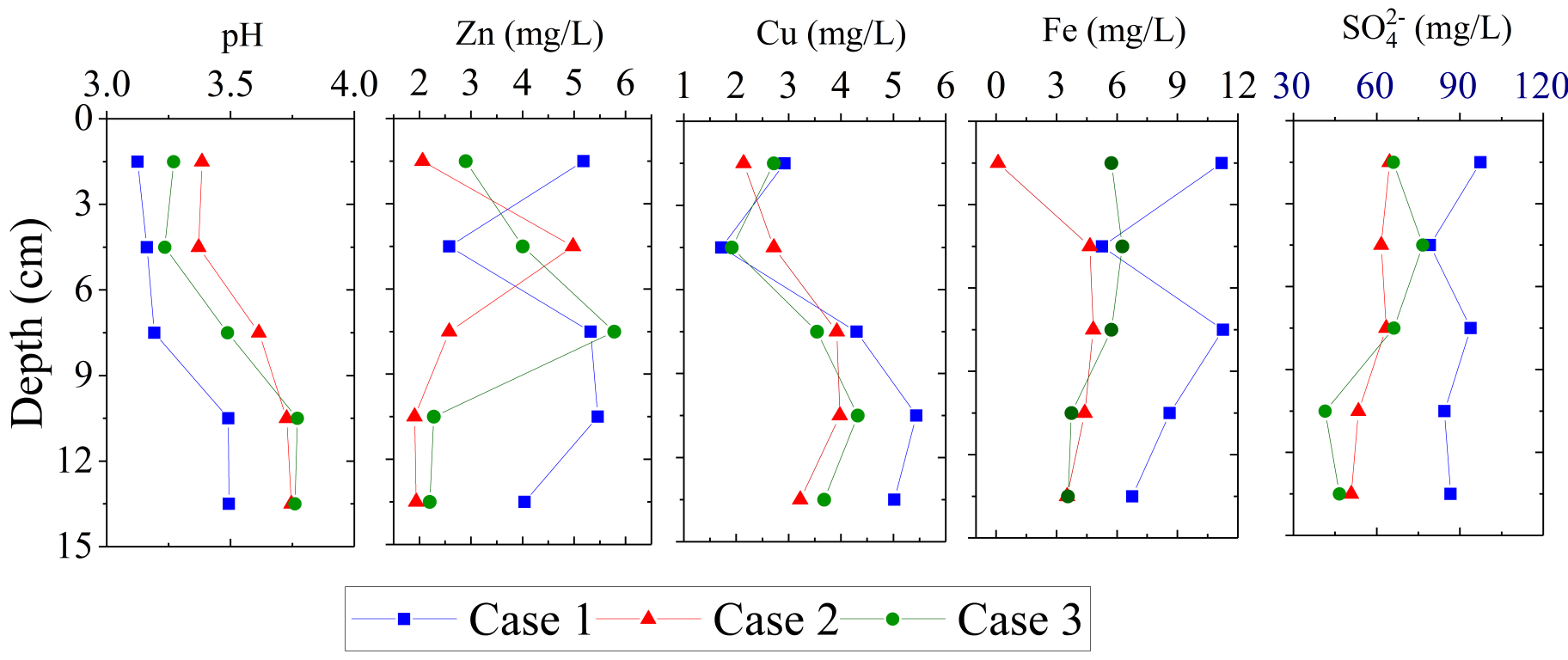
pH
3.0
3.5
4.0
Zn (mg/L)
2
3
4
5
6
Cu (mg/L)
1
2
3
4
5
6
Fe (mg/L)
0
3
6
9
12
SO_4^{2-} (mg/L)
30
60
90
120
Depth (cm)
0
3
6
9
12
15
Case 1
Case 2
Case 3

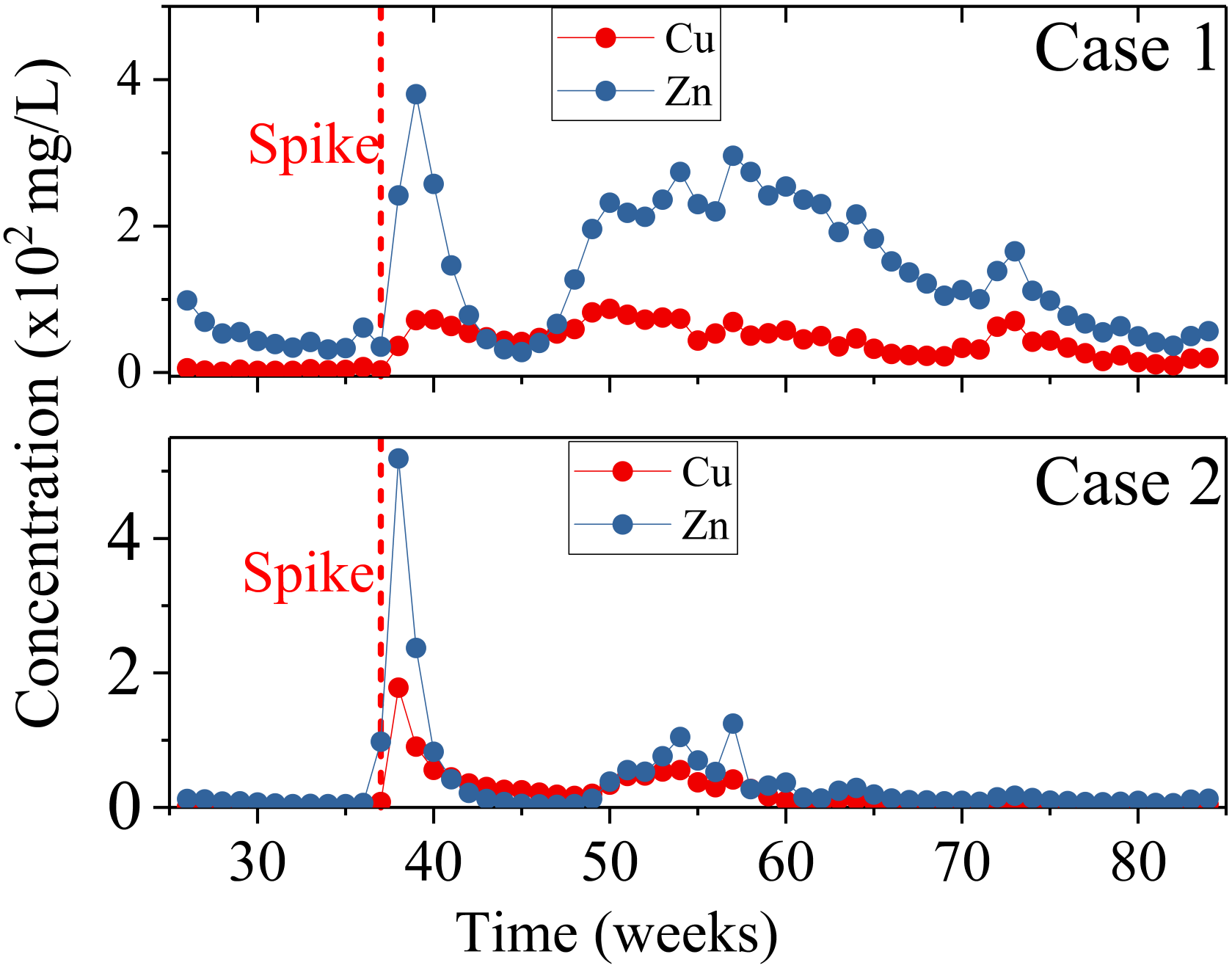
Case 1
Cu
Zn
Spike
Case 2
Cu
Zn
Spike
Concentration (x10^2 mg/L)
0
2
4
30
40
50
60
70
80
Time (weeks)

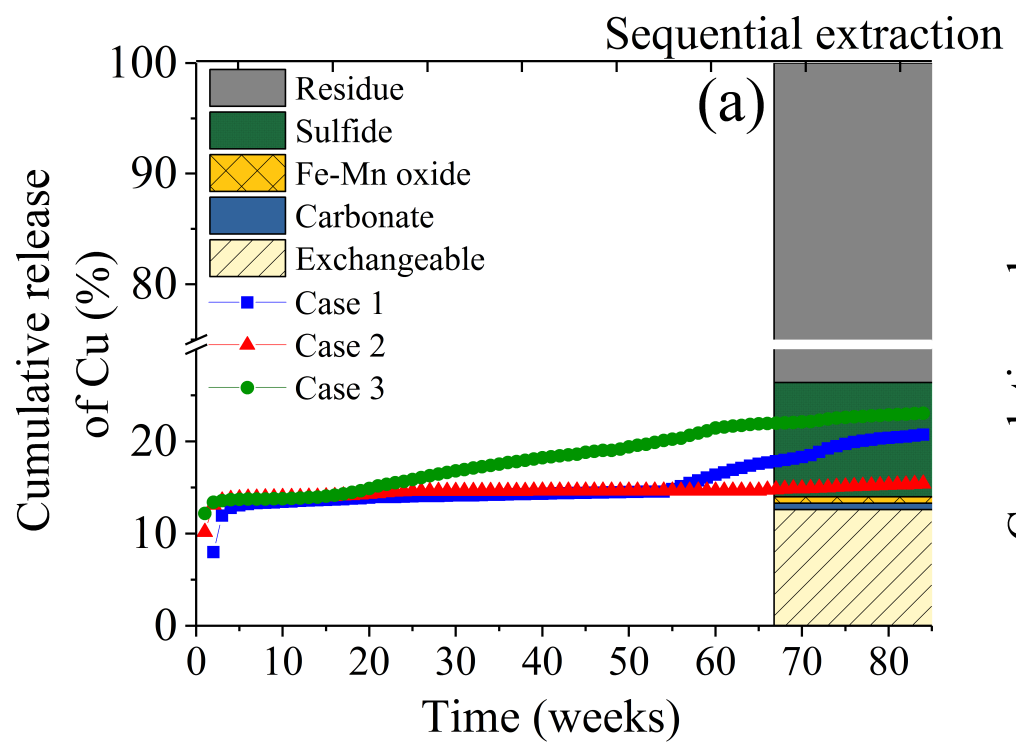
Sequential extraction
(a)
Residue
Sulfide
Fe-Mn oxide
Carbonate
Exchangeable
Case 1
Case 2
Case 3
Cumulative release of Cu (%)
Time (weeks)

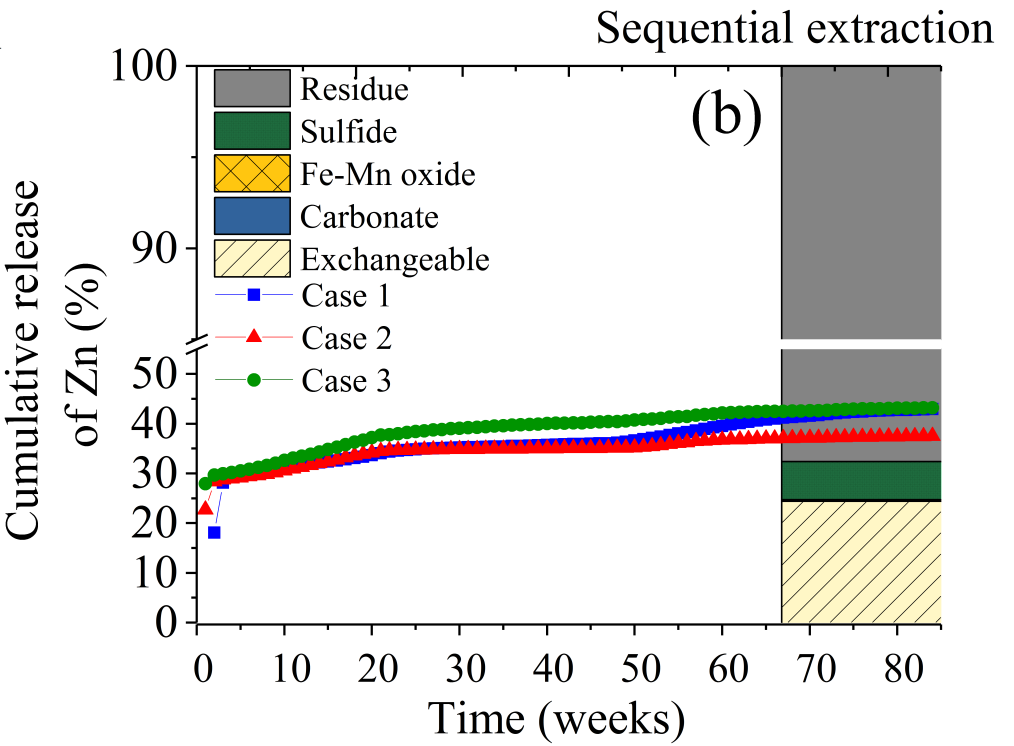
Sequential extraction
(b)
Residue
Sulfide
Fe-Mn oxide
Carbonate
Exchangeable
Case 1
Case 2
Case 3
Cumulative release of Zn (%)
Time (weeks)

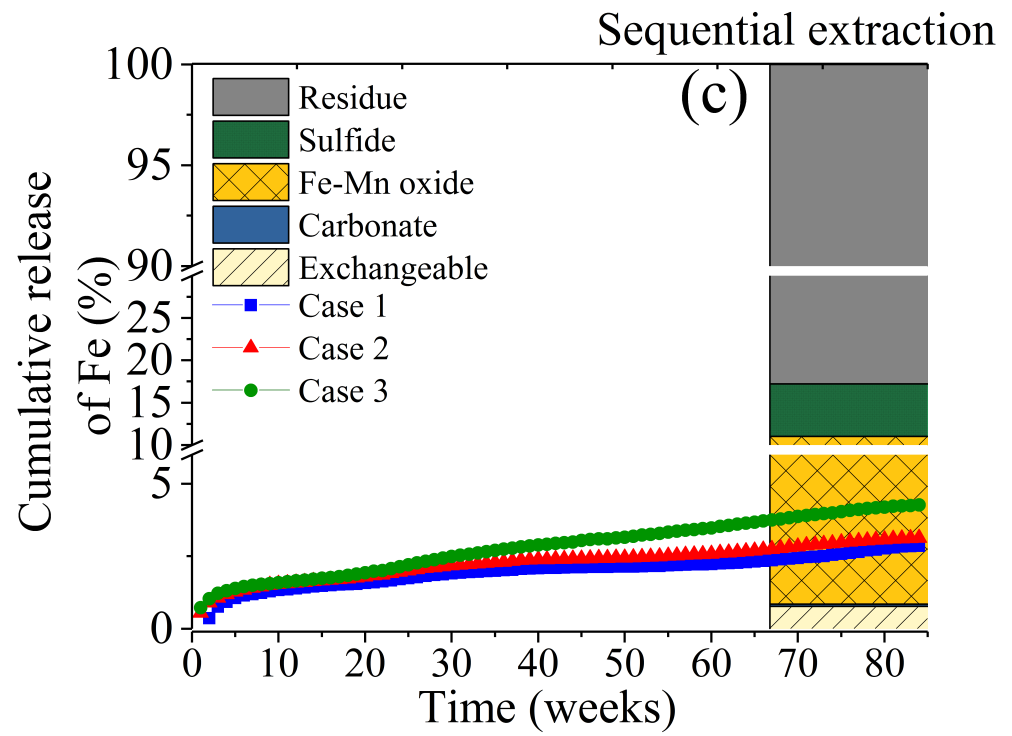
Sequential extraction
(c)
Residue
Sulfide
Fe-Mn oxide
Carbonate
Exchangeable
Case 1
Case 2
Case 3
Cumulative release of Fe (%)
Time (weeks)

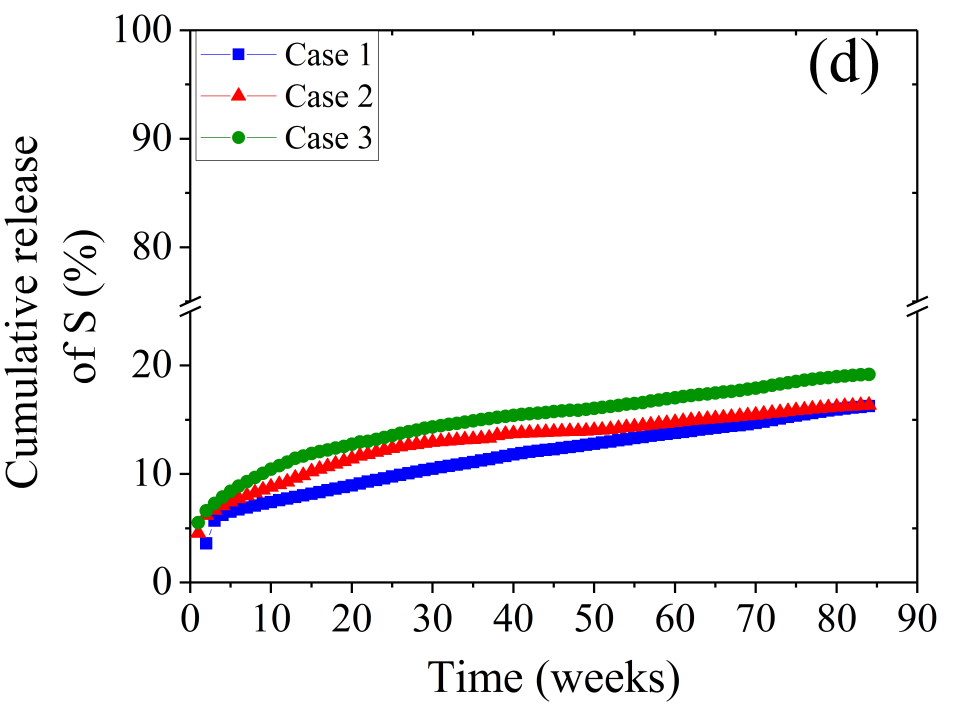
(d)
Case 1
Case 2
Case 3
Cumulative release of S (%)
Time (weeks)

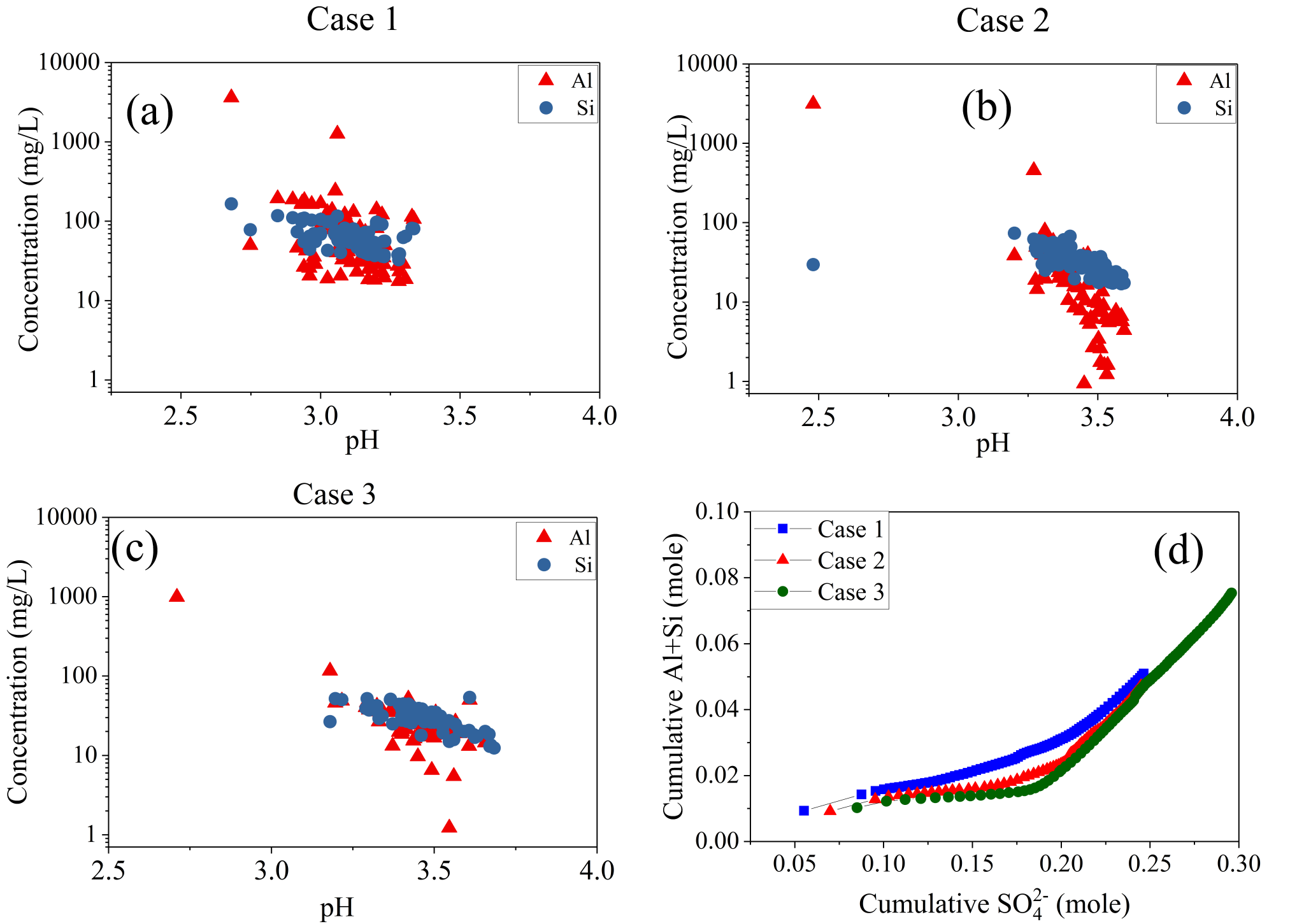
Case 1
Case 2
Case 3
(a)
(b)
(c)
(d)
Al
Si
Concentration (mg/L)
pH
Cumulative Al+Si (mole)
Cumulative SO_4^{2-} (mole)
Case 1
Case 2
Case 3

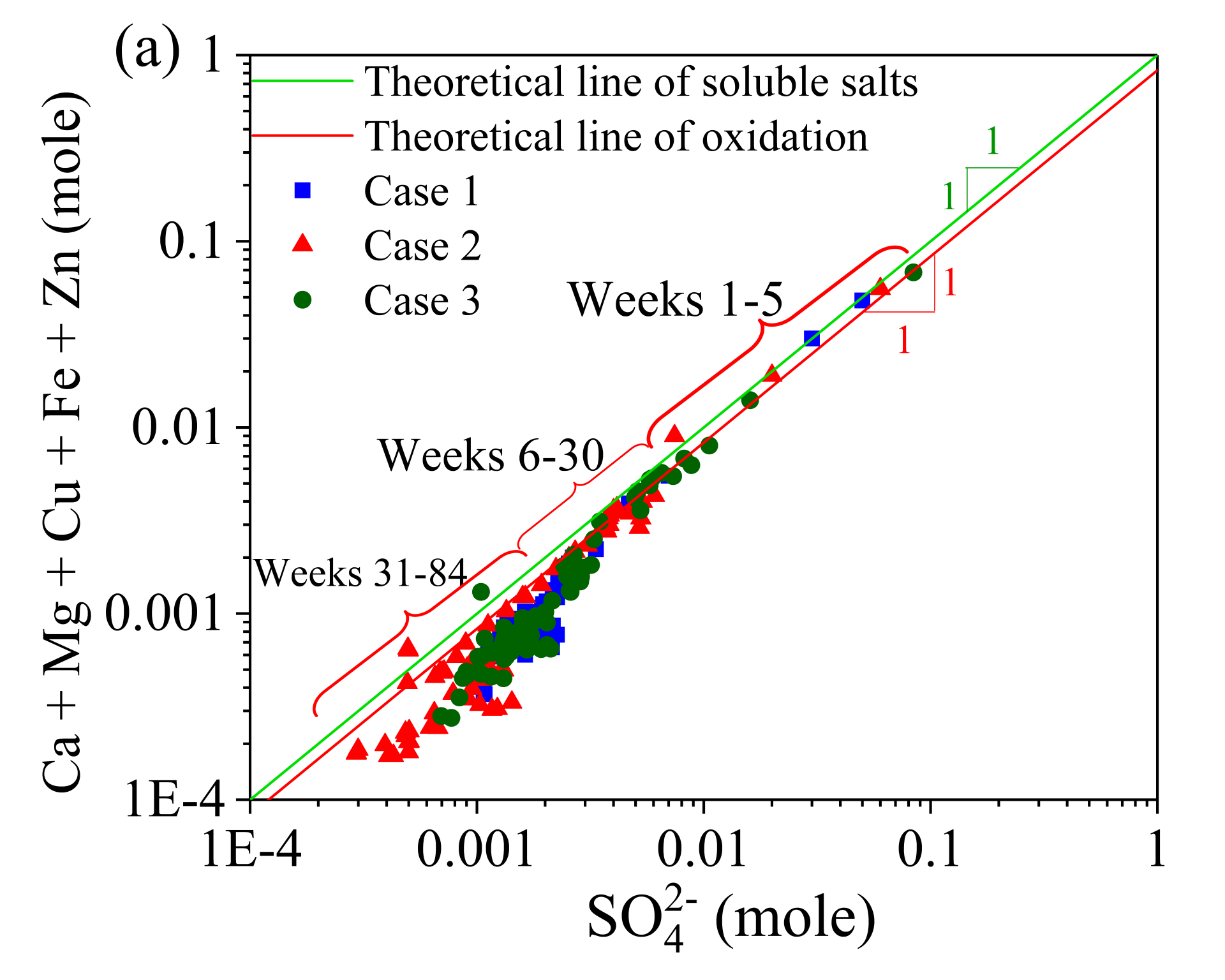
(a)
Theoretical line of soluble salts
Theoretical line of oxidation
Case 1
Case 2
Case 3
Weeks 1-5
Weeks 6-30
Weeks 31-84
1
1
1
1
1
0.1
0.01
0.001
1E-4
1E-4
0.001
0.01
0.1
1
Ca + Mg + Cu + Fe + Zn (mole)
SO_4^{2-} (mole)

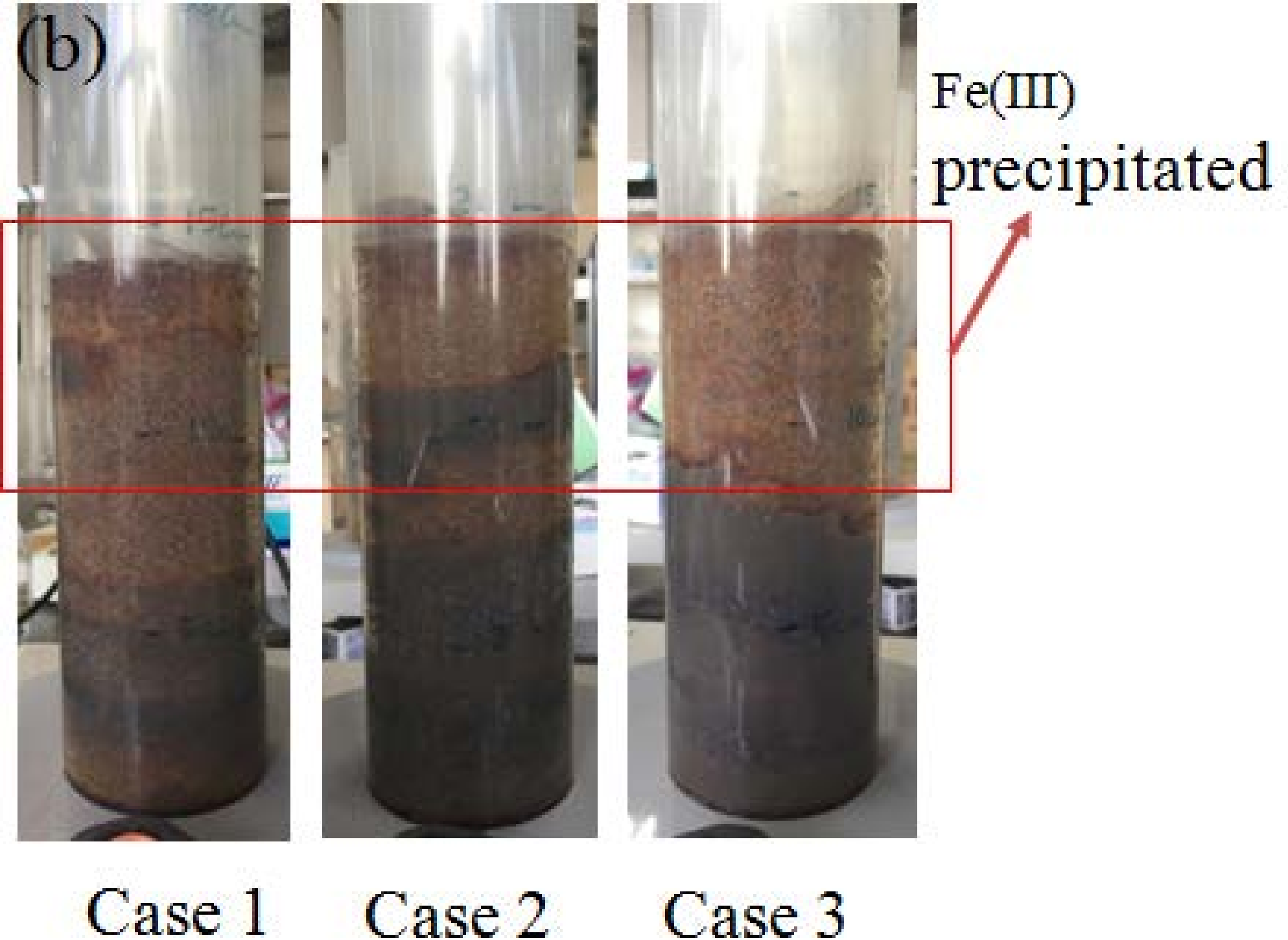
(b)
Fe(III)
precipitated
Case 1
Case 2
Case 3

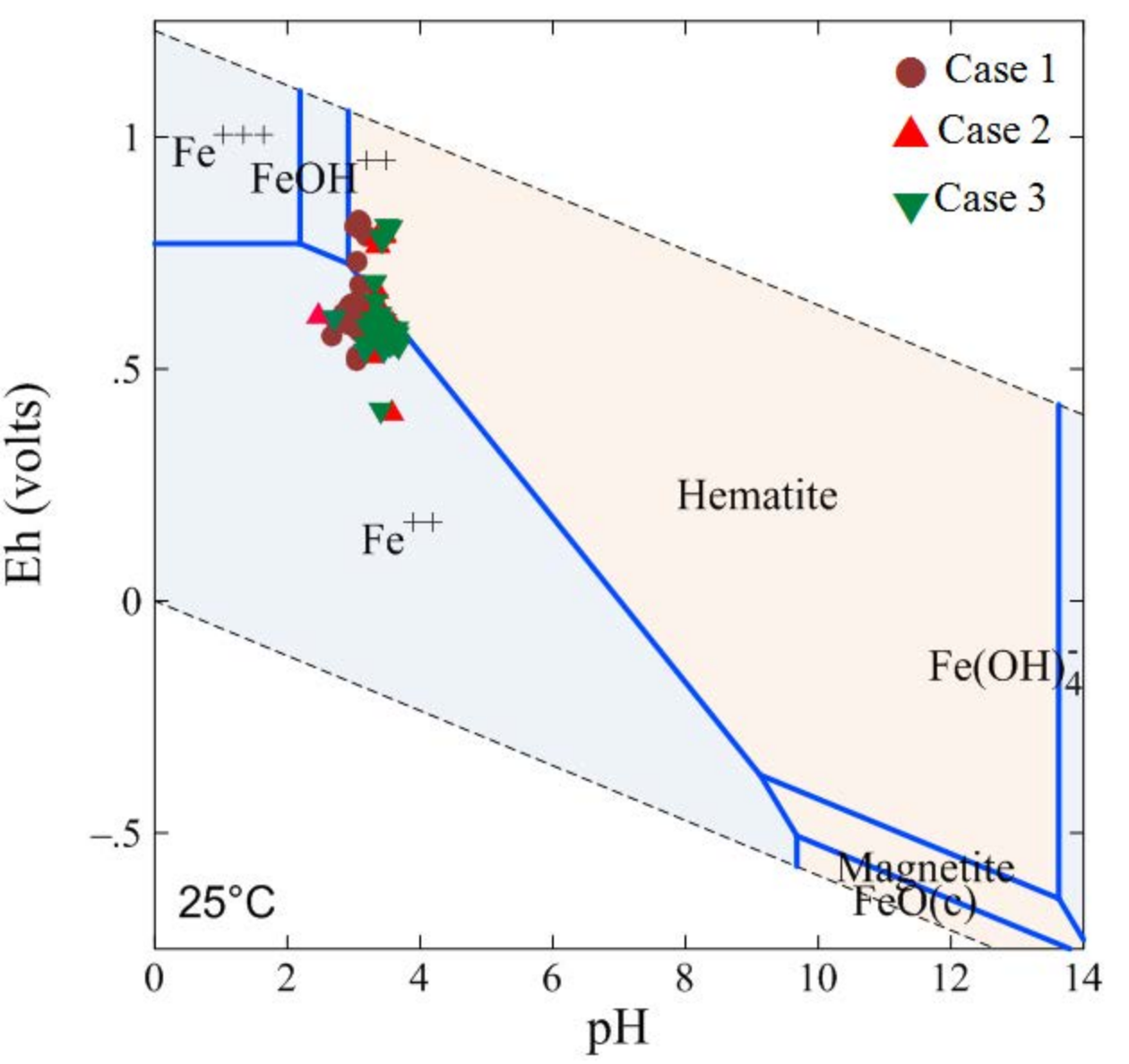
Case 1
Case 2
Case 3
Fe+++
FeOH++
Fe++
Hematite
Fe(OH)4-
Magnetite
FeO(c)
25°C
Eh (volts)
pH
1
.5
0
-.5
0
2
4
6
8
10
12
14